

Germline bias dictates cross-serotype reactivity in a common dengue virus-specific CD8⁺ T cell response

Abigail Culshaw^{1,13}, Kristin Ladell^{2,13}, Stephanie Gras^{3,4,13}, James E McLaren^{2,13}, Kelly L Miners², Carine Farenc^{3,4}, Heleen van den Heuvel³, Emma Gostick², Wanwisa Dejnirattisai¹, Apirath Wangteeraprasert^{1,11}, Thaneeya Duangchinda⁵, Pojchong Chotiyarnwong^{1,12}, Wannee Limpitikul⁶, Sirijitt Vasanawathana⁷, Prida Malasit⁸, Tao Dong⁹, Jamie Rossjohn^{2,3,4,14}, Juthathip Mongkolsapaya^{1,8,14}, David A Price^{2,10,14}, Gavin R Screaton^{1,14}

¹Department of Medicine, Imperial College London, London, UK; ²Institute of Infection and Immunity, Cardiff University School of Medicine, Cardiff, UK; ³Infection and Immunity Program and Department of Biochemistry and Molecular Biology, Biomedicine Discovery Institute, Monash University, Clayton, Victoria, Australia; ⁴Australian Research Council Centre of Excellence for Advanced Molecular Imaging, Monash University, Clayton, Victoria, Australia; ⁵Medical Biotechnology Unit, National Center for Genetic Engineering and Biotechnology, National Science and Technology Development Agency, Pathum Thani, Thailand; ⁶Pediatric Department, Songkhla Hospital, Ministry of Public Health, Songkhla, Thailand; ⁷Pediatric Department, Khon Kaen Hospital, Ministry of Public Health, Khon Kaen, Thailand; ⁸Dengue Hemorrhagic Fever Research Unit, Office for Research and Development, Faculty of Medicine, Siriraj Hospital, Mahidol University, Bangkok, Thailand; ⁹Medical Research Council Human Immunology Unit, Weatherall Institute of Molecular Medicine, University of Oxford, Oxford, UK; ¹⁰Human Immunology Section, Vaccine Research Center, National Institute of Allergy and Infectious Diseases, National Institutes of Health, Bethesda, Maryland, USA.

¹¹Current address: Naresuan University, Phitsanulok, Thailand.

¹²Current address: Department of Orthopaedic Surgery, Faculty of Medicine, Siriraj Hospital, Mahidol University, Bangkok, Thailand.

¹³These authors contributed equally to this work.

¹⁴These authors jointly directed this work.

Running title: TCR bias in dengue virus infection

Correspondence should be addressed to J.R. (jamie.rossjohn@monash.edu), J.M. (j.mongkolsapaya@imperial.ac.uk), D.A.P. (priced6@cardiff.ac.uk), or G.R.S. (g.screaton@imperial.ac.uk).

ABSTRACT

Adaptive immunity plays a key role in protection from dengue virus (DENV) infection, yet cross-reactivity with distinct serotypes can precipitate life-threatening clinical disease. We report that clonotypes expressing shared *TRBV11-2* gene rearrangements are preferentially activated and mobilized within the immunodominant human leukocyte antigen (HLA)-A*11:01-restricted NS3₁₃₃ epitope-specific CD8⁺ T cell response to DENV1 and DENV3/4. In contrast, the NS3₁₃₃ DENV2-specific repertoire is largely devoid of such T cell receptors (TCRs). Structural analysis of a representative TRBV11-2⁺ TCR demonstrated that cross-serotype reactivity is governed by a unique interplay between the variable antigenic determinant and germline-encoded residues in the second β -chain complementarity-determining region (CDR2 β). Extensive mutagenesis studies further confirmed that biophysical and functional engagement of three distinct TRBV11-2⁺ TCRs was highly dependent on key contacts between the serotype-defined peptide and discrete residues in the CDR2 β loop. Collectively, these data reveal an innate-like mode of epitope recognition with potential implications for the outcome of sequential exposure to heterologous DENVs.

INTRODUCTION

Dengue is endemic in tropical and sub-tropical regions of the world, causing up to 390 million infections annually with approximately 96 million cases of symptomatic disease and 25,000 deaths¹. Most clinically apparent infections result in a self-limiting febrile illness termed dengue fever. However, a minority of patients develop dengue haemorrhagic fever/dengue shock syndrome (DHF/DSS), a more serious manifestation characterized by vascular leakage and circulatory shock.

There are four serotypes of dengue virus (DENV1–4), which differ at the amino acid level by 30–35%. As a consequence of this heterogeneity, immunity to one serotype does not necessarily protect against infection with another serotype. Sequential infections are therefore common in dengue-endemic countries, where all four serotypes often circulate at the same time or replace each other in a cyclical manner. Epidemiological studies have further shown that adverse clinical outcomes are more frequent during secondary or recurrent infections. This key observation implicates adaptive immune responses in the pathogenesis of disease^{2,3}.

Antibody-dependent enhancement (ADE) is thought to provide the link between severe immunopathology and consecutive infection. The ADE hypothesis posits that antibodies generated in response to the initial serotype will fail to neutralize subsequent viruses, yet still bind with sufficient avidity to enhance viral replication via Fc receptor-mediated uptake into myeloid cells⁴. This process has been demonstrated *in vitro*^{5,6} and in animal models^{7,8,9}. In addition, higher virus loads driven by ADE correlate with disease severity¹⁰. However, the vascular leak that occurs during DHF/DSS tends to develop when the fever remits, which coincides with a steep fall in virus load and an inflammatory “cytokine storm”. This temporal association between symptomatic disease and viral clearance suggests a pathogenic role for DENV-specific T cells.

Non-structural protein-3 (NS3) is classically described as the immunodominant T cell antigen in DENV^{11,12}. Comprehensive approaches have largely substantiated these initial observations and further enabled the identification of many other targeted epitopes across

the entire viral proteome¹³. Virus-specific CD4⁺ and CD8⁺ T cells are highly activated during acute infection, and the magnitude of the overall response correlates with disease severity¹². There is also good evidence to support a protective role for DENV-specific T cells in humans¹³ and mouse models^{14, 15}. Accordingly, the lack of a potent T cell immunogen may explain the relatively poor efficacy of a chimeric vaccine designed to elicit neutralizing antibodies against the precursor membrane and envelope proteins from DENV1–4¹⁶.

To clarify the mechanisms that underpin this dichotomy between pathogenesis and protection, we conducted a detailed investigation of NS3₁₃₃ DENV-specific CD8⁺ T cell responses in a cohort of patients from Thailand. Restricted by human leukocyte antigen (HLA)-A*11:01, which occurs in this population with an allelic frequency of approximately 30%¹⁷, the NS3₁₃₃ epitope is typically immunodominant and can elicit secondary responses comprising up to 10–12% of the circulating CD8⁺ T cell pool¹⁸. A number of sequence variants have also been described, leading to distinct patterns of cross-serotype reactivity that potentially affect disease outcome¹⁹. The data presented here reveal that serotype-defined epitope cross-recognition is driven by a previously unknown mode of antigen engagement involving direct interactions between the NS3₁₃₃ peptide and germline-encoded residues in the second β -chain complementarity-determining region (CDR2 β) that characterize a highly biased subset of T cell receptors (TCRs). Key components of the adaptive repertoire are therefore inherited at the *TRBV* gene locus, ensuring common and predictable immune reactivity against various circulating strains of DENV.

RESULTS

Cross-serotype TCR bias in NS3₁₃₃ DENV-specific CD8⁺ T cell populations

To investigate the molecular basis of cross-reactivity within the immunodominant NS3₁₃₃ DENV-specific CD8⁺ T cell response, we first generated HLA-A*11:01-peptide (HLA-A*11:01p) tetramers corresponding to the most prevalent epitope variant (GTS1, GTS2, or GTS3/4) for each serotype (DENV1–4) among viral isolates from Thailand (Fig. 1a). These reagents were used in conjunction with polychromatic flow cytometry to quantify and sort antigen-specific CD8⁺ T cell populations directly *ex vivo* from the peripheral blood of patients infected with DENV (Supplementary Table 1). A single HLA-A*11:01p tetramer was used in cases of primary infection, matched to the gene-identified serotype determined by RT-PCR. Two HLA-A*11:01p tetramers with distinct fluorochrome tags were used simultaneously in cases of secondary infection, matched to the recently encountered serotype and the primary serotype determined on the basis of micro-focus reduction neutralization tests (micro-FRNTs). Representative flow cytometry plots are shown in Fig. 1b. An unbiased molecular approach was then used to characterize all expressed *TRB* gene rearrangements in each sorted HLA-A*11:01p tetramer-defined CD8⁺ T cell population (Supplementary Figs. 1–5).

Preferential usage of the *TRBV11-2* gene was apparent in NS3₁₃₃ DENV-specific CD8⁺ T cell populations targeting the GTS1 and GTS3/4 variants (Fig. 1c). The *TRBV9* and *TRBV12-3/4* genes were also favoured during infections with DENV1 and DENV3/4. In contrast, these germline transcripts were rarely detected in GTS2-specific CD8⁺ T cell populations. Further inspection of the biased repertoires associated with HLA-A*11:01-GTS1 and HLA-A*11:01-GTS3/4 revealed centrally located glycines in the somatically rearranged CDR3 β loop and preservation of the *TRBV* gene-encoded leucine at position 5. Eight amino acid residue-identical TCR β sequences were present in more than one patient infected with the corresponding serotypes (DENV1/3/4). Six of these “public” sequences incorporated

TRBV11-2 (Supplementary Table 2), and all were variously encoded across the junctional region (Supplementary Fig. 6).

To confirm these patterns of epitope-specific bias at the protein level, we used serotype-matched HLA-A*11:01p tetramers and a TRBV11-2-specific mAb to stain peripheral blood mononuclear cells (PBMCs) from 23 additional patients with secondary infection (Supplementary Table 3). Representative flow cytometry plots are shown in Fig. 1d. Antigen-specific usage of TRBV11-2 was significantly more common in CD8⁺ T cell populations targeting the GTS1 and GTS3/4 epitopes compared with CD8⁺ T cell populations targeting the GTS2 epitope (Fig. 1e). Cross-staining of TRBV11-2⁺ clonotypes with the HLA-A*11:01-GTS1 and HLA-A*11:01-GTS3/4 tetramers was also observed during primary infection (data not shown). Collectively, these data show that the serotype-defined epitope sequence dictates germline bias in the NS3₁₃₃ DENV-specific TCR repertoire.

Characterization of representative TRBV11-2⁺ NS3₁₃₃ DENV-specific CD8⁺ T cell clones

To examine variant cross-recognition in the context of epitope-dependent TCR bias, we generated a panel of NS3₁₃₃ DENV-specific CD8⁺ T cell clones. Functionality was assessed in response to HLA-matched B-lymphoblastoid cell lines pulsed separately with exogenous peptides corresponding to GTS1, GTS2, and GTS3/4. Distinct effector readouts were measured independently and simultaneously using polychromatic flow cytometry (Fig. 2a). Clones OX17 2H, 44-173 13, and 44-173 30, all of which express TRBV11-2, preferentially recognized GTS1 and GTS3/4. A similar pattern of activation was observed with the TRBV12-3/4⁺ clone N15 22. In contrast, the TRBV12-3/4⁺ clone 44-038 25 and the TRBV7-6⁺ clone E5 responded maximally to all three peptide variants, whereas the TRBV2⁺ clone D9 became less polyfunctional according to the hierarchy GTS3/4 > GTS2 > GTS1. These data confirm that TRBV11-2 usage is associated with enhanced recognition of GTS1 and GTS3/4.

Molecular analysis of the rearranged *TRB* gene transcripts from clones OX17 2H, 44-173 13, and 44-173 30 revealed features consistent with the *ex vivo* data, including a

CASSLGXG motif in the CDR3 β loop (Fig. 2b). Each TCR β -chain paired with a distinct TCR α -chain. To determine the biophysical correlates of differential epitope recognition, we refolded the corresponding heterodimeric TCRs *in vitro* and undertook surface plasmon resonance (SPR) binding measurements with soluble HLA-A*11:01p complexes (Table 1 and Supplementary Fig. 7). The OX17 2H TCR (termed D2H from hereon) displayed high affinity interactions with HLA-A*11:01-GTS1 and HLA-A*11:01-GTS3/4 ($K_{Deq} < 10 \mu\text{M}$) and a low affinity interaction with HLA-A*11:01-GTS2 ($K_{Deq} > 200 \mu\text{M}$). In contrast, the 44-173 13 TCR (termed D13 from hereon) bound very weakly to all three HLA-A*11:01p complexes ($K_{Deq} > 400 \mu\text{M}$). These are remarkably low affinities for a naturally selected pathogen-specific TCR^{20, 21}. Accurate measurements within this range were precluded by technical constraints, but the relative K_{Deq} values presumably mirror the slight functional differences observed at the clonal level. The 44-173 30 TCR (termed D30 from hereon) bound weakly to HLA-A*11:01-GTS1 and HLA-A*11:01-GTS3/4 ($K_{Deq} \sim 150 \mu\text{M}$) and very weakly to HLA-A*11:01-GTS2 ($K_{Deq} > 400 \mu\text{M}$). These data are consistent with the activation profiles shown in Fig. 2a.

Serotype-defined NS3₁₃₃ DENV peptides are presented similarly by HLA-A*11:01

To determine how C-terminal amino acid mutations in the bound epitope affect TRBV11-2⁺ TCR-mediated antigen recognition, we first used a thermal shift assay to measure the stability of each binary HLA-A*11:01p complex. No significant differences in melting point (T_M) were detected between HLA-A*11:01-GTS1 ($T_M = 61.6 \pm 0.8 \text{ }^\circ\text{C}$), HLA-A*11:01-GTS2 ($T_M = 62.7 \pm 0.7 \text{ }^\circ\text{C}$), and HLA-A*11:01-GTS3/4 ($T_M = 62.3 \pm 1.0 \text{ }^\circ\text{C}$). These data indicate that all three serotype-defined variants of NS3₁₃₃ are readily accommodated by HLA-A*11:01. We then solved the crystal structures of HLA-A*11:01-GTS1 and HLA-A*11:01-GTS3/4 (Fig. 2c–e and Table 2). The structures of HLA-A*11:01-GTS1 and HLA-A*11:01-GTS3/4 were very similar, with a root mean square deviation (r.m.s.d.) of 0.34 Å for the overall complex (Fig. 2e). In each case, the P2-Thr and P10-Arg were buried inside the

antigen-binding cleft, acting as anchor residues, while the central region of the peptide from P4-Gly to P9-Asn was solvent exposed. The shared P5-Ser and P6-Pro were highly mobile. This close structural homology reflects the fact that GTS1 and GTS3/4 differ by a single residue, namely the conservative switch from P8-Val (DENV1) to P8-Ile (DENV3/4). In contrast, GTS2 contains a P9-Asp in place of P9-Asn. Collectively, these data suggest that specific TCR-mediated contacts with the HLA-A*11:01-bound peptide, likely focused on the neutral Asn residue at P9, underpin the preferential deployment of TRBV11-2 in response to NS3₁₃₃ DENV1/3/4.

HLA-A*11:01-GTS1/3/4 recognition is dominated by TCR β

To define the molecular basis of serotype-restricted bias in the NS3₁₃₃ DENV-specific CD8⁺ T cell response, we solved the ternary structures of HLA-A*11:01-GTS1 and HLA-A*11:01-GTS3/4 in complex with the D30 TCR (Table 2). The electron density at the TCR-HLA-A*11:01p interface was unambiguous in each case, permitting a detailed analysis of the interactions with GTS1 and GTS3/4.

The D30 TCR docked similarly on top of both HLA-A*11:01p complexes (r.m.s.d. of 0.6 Å), with the center of mass towards the N-terminal region of the peptide (Fig. 3a,b). The overall buried surface area (BSA) fell within the normal range at $\sim 1850 \text{ \AA}^2$ ²¹. Contacts between the TCR α -chain and HLA-A*11:01p were limited to a few residues in each ternary complex (31% of the BSA). The CDR1 α loop sat above the N-terminal region of the antigen-binding cleft, acting as a “lid” over P1-Gly (Fig. 4a), while interacting solely with Arg163 in the α 2-helix of HLA-A*11:01 via a hydrogen bond and van der Waals contacts (Supplementary Table 4). The CDR3 α loop also interacted with HLA-A*11:01 via a smattering of van der Waals contacts, together with hydrogen bonds and a salt bridge between Asp109 α and residues Gln62 and Arg65, respectively, in the α 1-helix (Fig. 4b and Supplementary Table 4). In contrast, the β -chain contributed 69% of the BSA. This interaction was driven predominantly by CDR3 β (34% of the BSA), CDR2 β (22% of the BSA), and FW β (11% of the BSA), placing the D30 TCR complexes with HLA-A*11:01-GTS1

and HLA-A*11:01-GTS3/4 among the most β -centric ternary structures reported to date^{21, 22,}

23

The CDR2 β loop and the downstream framework residues Val66 β and Asp67 β interacted with residues 65–76 in the α 1-helix of HLA-A*11:01, while the β -hairpin shape of the CDR2 β -FW β segment sat parallel above the α 1-helix, maximizing contact with the HLA-A*11:01 molecule (Fig. 4c). These interactions were mediated largely by van der Waals contacts (Supplementary Table 4). The CDR3 β loop interacted with HLA-A*11:01 primarily via the α 2-helix, while also stretching across the antigen-binding cleft to contact Ala69 in the α 1-helix (Fig. 4d). Of particular note, the aromatic group of Tyr114 β was inserted between the peptide and the hinge of the α 2-helix, forming hydrogen bonds with Ala150 and Gln155. Accordingly, the D30 TCR interacts with HLA-A*11:01-GTS1 and HLA-A*11:01-GTS3/4 mainly via the β -chain, with dominant contributions from CDR2 β -FW β and CDR3 β .

TRBV11-2 bias is driven by serotype-defined NS3₁₃₃ DENV peptides

The GTS1 and GTS3/4 peptides both contributed 24% of the BSA, which falls within the normal range established by previous studies²¹. Each peptide also interacted similarly with the D30 TCR (Supplementary Table 4). Interactions with the α -chain were limited to a few contacts between the CDR3 α loop and residues P4-Gly and P5-Ser. In contrast, the CDR3 β loop sat above the central hydrophobic region of the peptide (⁴GSPV/I⁸), dominating the overall interaction between the TCR and GTS1/3/4 (Fig. 4e and Supplementary Fig. 8).

The central region of each peptide showed a degree of mobility in the binary HLA-A*11:01p structure, but adopted a more stable conformation after TCR engagement to sit deeper in the antigen-binding cleft (Supplementary Fig. 9). In the ternary structures, the P5-Ser C α and the P6-Pro C α of the GTS1 peptide shifted by 2.3 Å and 1.2 Å, respectively (peptide r.m.s.d. of 0.78 Å), while the P5-Ser C α and the P6-Pro C α of the GTS3/4 peptide shifted by 1.5 Å and 1 Å, respectively (peptide r.m.s.d. of 0.59 Å). This conformational change was due to extensive peptide interactions with the CDR3 β loop, the majority of which were main chain-main chain contacts (Fig. 4e, Supplementary Fig. 8, and Supplementary

Table 4). In contrast, most of the CDR3 β side chains were pushed outside the antigen-binding cleft to mediate specific contacts with the HLA-A*11:01 molecule. These findings are somewhat reminiscent of a previous report in which TCR recognition was dependent on the length rather than the amino acid sequence of the CDR3 β loop²⁴.

The CDR2 β loop engaged GTS1 and GTS3/4 via side chain-mediated interactions, providing a structural explanation for the observed peptide-dependent TRBV11-2 bias (Fig. 4f and Supplementary Fig. 8). Specifically, Gln57 β hydrogen bonded with the backbone of P7-Ile, while Asn58 β formed a double hydrogen bond with the side chain of P9-Asn (Fig. 4f and Supplementary Table 4). The importance of Asn58 β was reinforced by further analysis of the *ex vivo* NS3₁₃₃ DENV-specific TCR β sequences, which revealed substantially higher proportions of Asn58 β ⁺ clonotypes in the HLA-A*11:01-GTS1/3/4-specific repertoires compared with the HLA-A*11:01-GTS2-specific repertoires (Fig. 5a,b). In addition, Asn58 β ⁺ TRBV segments with a charged amino acid at position 59 were poorly represented in the overall dataset, barring TRBV7-8. These observations link conceptually with the finding that antigen recognition can be impaired by single-residue allelic polymorphisms in the vicinity of the CDR2 β loop²⁵.

Peptide interactions with the CDR2 β loop are required for TRBV11-2⁺ TCR-mediated recognition of HLA-A*11:01-GTS1/3/4

To define the key residues that underpin antigen-specific usage of TRBV11-2, we conducted alanine/glycine scanning mutagenesis experiments to probe “energetic hotspots” at the D30 TCR-HLA-A*11:01-GTS1 interface. Single point substitutions were designed using the ternary crystal structure as a guide, and each alanine/glycine-substituted mutant was expressed, refolded, and purified in a standardized manner. Thirteen individual substitutions were introduced into the D30 TCR β -chain (Supplementary Table 5). Of these mutants, only the Tyr114 β Ala TCR failed to refold, precluding further analysis. The control Leu81 β Ala mutation did not affect TCR binding to HLA-A*11:01-GTS1 (Fig. 6a). Similarly,

residue substitutions in the CDR1 β loop were tolerated with minimal changes in the overall interaction affinity, as determined using SPR (Fig. 6a, Supplementary Fig. 10, and Supplementary Table 5). In contrast, mutations at positions 108–112 in the CDR3 β loop, aligned with the central footprint on the surface of the HLA-A*11:01p complex, and mutations at Gln57 β and Asn58 β , which interacted predominantly with the peptide residues P7-Ile and P9-Asn, respectively, either abrogated or substantially diminished TCR binding to HLA-A*11:01-GTS1 (Fig. 6a, Supplementary Fig. 10, and Supplementary Table 5). These results identify a continuous energetic hotspot that runs across the central axis of the D30 TCR (Fig. 6a).

In reciprocal experiments, we generated single alanine-substituted mutants of HLA-A*11:01-GTS1 to define the corresponding energetic landscape and determine the extent to which interaction hotspots are conserved across different TRBV11-2⁺ TCRs (Supplementary Fig. 11 and Supplementary Table 6). Four residues were mutated in the α 1-helix of HLA-A*11:01 (Arg65, Lys68, Gln72, and Val76), and two residues were mutated in the α 2-helix of HLA-A*11:01 (Arg145 and Gln155). A third residue in the α 2-helix was mutated as a control (Arg154). In addition, we investigated the effect of amino acid substitutions at P5-Ser and P9-Asn in the GTS1 peptide. All of these mutant proteins were stable (Supplementary Table 7). Common hotspots on the HLA-A*11:01-GTS1 complex were apparent for the D2H, D13, and D30 TCRs (Fig. 6b–d). For example, mutations at Arg65 and Lys68 in the α 1-helix of HLA-A*11:01 negatively impacted binding of the D13 and D30 TCRs, while mutations at Arg65 in α 1-helix and Gln155 in the α 2-helix of HLA-A*11:01 similarly impacted binding of the D2H and D30 TCRs. The corresponding mutant HLA-A*11:01-GTS1 tetramers displayed analogous staining patterns in titration experiments with the parental NS3₁₃₃ DENV-specific CD8⁺ T cell clones (Supplementary Fig. 12a). These findings indicate that a consensus footprint underpins TRBV11-2⁺ TCR-mediated recognition of HLA-A*11:01-GTS1. Of note, the mutation at Gln72 enhanced binding of the D13 and D30 TCRs to HLA-A*11:01-GTS1 (Fig. 6b,c, Supplementary Fig. 11, and Supplementary Table 6). A similar effect was

observed with the Asn59 β Ala mutant D30 TCR (Supplementary Fig. 10 and Supplementary Table 5). In the corresponding ternary structure, Gln72 interacted with Asn59 β in the CDR2 β loop (Fig. 6e). It therefore seems likely that the respective alanine substitutions allow more intimate contacts between the CDR2 β loop and HLA-A*11:01-GTS1.

Alanine substitution of P9-Asn dramatically reduced binding of the D2H, D13, and D30 TCRs to HLA-A*11:01-GTS1 (Fig. 6b–e, Supplementary Fig. 11, and Supplementary Table 6). Similarly, replacement of P9-Asp with aspartic acid, a negatively charged residue that occurs naturally in the GTS2 peptide, abrogated binding of the D2H, D13, and D30 TCRs to HLA-A*11:01-GTS1. Analogous effects were observed in functional assays with the parental NS3₁₃₃ DENV-specific CD8⁺ T cell clones (Fig. 6f and Supplementary Fig. 12b,c). Collectively, these data show that P9-Asn acts as a common hotspot for TRBV11-2⁺ TCRs within a conserved footprint on the surface of HLA-A*11:01-GTS1.

DISCUSSION

In this study, we investigated the phenomenon of cross-serotype reactivity within the immunodominant HLA-A*11:01-restricted NS3₁₃₃ DENV-specific CD8⁺ T cell response. The key findings were: (i) TRBV11-2⁺ clonotypes are preferentially recruited during infections with DENV1 and DENV3/4; (ii) CD8⁺ T cell clones expressing TRBV11-2⁺ TCRs recognize the corresponding HLA-A*11:01-restricted peptides GTS1 and GTS3/4 more efficiently compared with GTS2; (iii) TRBV11-2⁺ TCRs engage HLA-A*11:01-GTS1 and HLA-A*11:01-GTS3/4 with higher affinities relative to HLA-A*11:01-GTS2; and (iv) TCR bias in the NS3₁₃₃ DENV-specific CD8⁺ T cell repertoire is governed by specific contacts between the germline-encoded CDR2 β loop and the serotype-defined peptides GTS1 and GTS3/4.

The ternary structures of HLA-A*11:01-GTS1 and HLA-A*11:01-GTS3/4 in complex with the TRBV11-2⁺ D30 TCR revealed that Asn58 β in the CDR2 β loop hydrogen bonds with the peptide residue P9-Asn. In addition, the TRBV11-2 segment perfectly complements these serotype-defined peptides, because the CDR2 β loop provides a neutral surface that facilitates docking with the neutral C-terminus of GTS1 and GTS3/4. The key P9-Asn residue is not present in GTS2, which instead contains a negatively charged P9-Asp. Alanine scanning mutagenesis experiments with the D30 TCR confirmed the importance of Asn58 β in the overall interaction with HLA-A*11:01-GTS1. Reciprocal studies with mutant HLA-A*11:01-GTS1 molecules further demonstrated a common footprint for three distinct TRBV11-2⁺ TCRs, all of which exhibited an absolute dependence on CDR2 β -mediated contacts with P9-Asn. Accordingly, TRBV11-2 is preferentially incorporated in the NS3₁₃₃ DENV1/3/4-specific CD8⁺ T cell repertoire as a function of peptide-driven contacts with germline-encoded regions of the TCR.

It is notable that other TRBV segments were commonly represented in the HLA-A*11:01-restricted CD8⁺ T cell populations specific for GTS1 (TRBV9, TRBV12-3/4, and TRBV27) and GTS3/4 (TRBV4-1, TRBV9, and TRBV12-3/4). Indeed, TRBV11-2 and TRBV12-3/4 were expressed by > 50% of all clonotypes mobilized in response to GTS1 and GTS3/4. The CDR2 β loops of TRBV11-2 (⁵⁶FQNGV⁶¹) and TRBV12-3/4 (⁵⁶FNNV⁶¹) are

similar and share the key Asn58 β residue that interacts directly with P9-Asn. Remarkably, Asn58 β is also present in TRBV9 (⁵⁶YYNGEE⁶¹) and TRBV27 (⁵⁶SMNVEV⁶¹). A peptide-specific “mosaicism” therefore exists within the selected germline-encoded CDR2 β loops. Such mosaics have only been observed previously for somatically rearranged components of the TCR²⁶.

Asn58 β is also present in TRBV segments that are rarely selected in response to GTS1 and GTS3/4, including TRBV7-9, TRBV11-3, TRBV12-5, and TRBV23-1. All of these “neglected genes” encode CDR2 β loops with a charged residue at position 59 (Arg or Glu). This observation is likely explained by the neutral surface around P9-Asn and adjacent residues in the HLA-A*11:01 molecule (Thr73–Val76). The exquisite specificity of TCR recognition focused on this area of the HLA-A*11:01p complex is further substantiated by the relative paucity of Asn58 β ⁺ clonotypes in the corresponding GTS2-specific repertoires, which were dominated individually by TRBV4-1⁺ (⁵⁷YSYEKL⁶¹) and TRBV5-1⁺ (⁵⁷YFSETQ⁶¹) TCRs.

It should be noted that our findings do not imply a universal “peptide sensing” role for the *TRBV11-2* gene-encoded CDR2 β loop. Indeed, a number of studies have reported that the CDR2 β loop can adopt different configurations to engage other HLA class I-restricted peptides recognized by TRBV11-2⁺ TCRs²¹. Similarly, descriptions of “interaction codons” in mice that pair certain major histocompatibility complex (MHC) allotypes with V α 3-3 or V β 8-2^{27, 28} do not predicate fixed rules of engagement for germline-encoded regions of the TCR²⁹. Diverse recognition modes can also be anticipated on philosophical grounds, considering the limited number of *TRAV/TRBV* genes and the vast array of potential antigens and MHC class I/II molecules.

In outbred human populations, a complex interplay between host genetics and viral diversity, overlaid by the phenomenon of sequential infection with distinct serotypes, convolutes associative studies of disease outcome. Several correlates have nonetheless been identified in different parts of the world. For example, in South-East Asia, severe disease has been linked with *HLA-A*0:07*, *HLA-A*24*, *HLA-A*31*, and *HLA-B*53*, while protection has been linked with *HLA-A*03*, *HLA-B*18*, and the *HLA-B*44* supertype^{30, 31, 32, 33}.

^{34, 35}. There is also evidence that sequential patterns of infection can predispose to serious clinical manifestations. For example, in Cuba, severe disease has been observed in secondary infections with DENV2 or DENV3 following primary infection with DENV1^{3, 36, 37}. More complicated scenarios have been reported in Nicaragua, where secondary infection with DENV2 clade NI-1, but not DENV2 clade NI-2B, causes severe disease in individuals with pre-existing immunity to DENV1³⁸. However, it remains to be determined to what extent cross-serotype reactivity in the memory T cell pool is associated with enhanced protection or a greater risk of immunopathology in the setting of recurrent DENV infection^{12, 13, 19, 39}.

In summary, the data presented here reveal a novel mechanism of TCR bias, whereby serotype-defined epitope recognition is “hard-wired” into the human genome. This key finding demonstrates that germline-encoded residues can dictate the cross-reactivity profile of individual clonotypes targeting a variable antigenic determinant and potentially explains the lack of a reproducible correlation between clinical outcome and the magnitude of the NS3₁₃₃ DENV-specific CD8⁺ T cell response^{18, 19, 40, 41}.

METHODS

Study population

Samples of venous blood were collected from DENV-infected patients at serial time points during acute infection and convalescence. Approval was granted by the Ethics Committees at Khon Kaen, Songkhla, and Siriraj Hospitals (Thailand), and by the Riverside Research Ethics Committee (UK). Informed consent was obtained in all cases. PBMCs and serum were isolated using density gradient centrifugation and cryopreserved according to standard protocols. The infecting serotype was identified using a DENV gene-based RT-PCR⁴². Secondary infection was defined as a DENV-specific IgM:IgG ratio < 1.8 in capture ELISAs⁴³. The infection history of each patient was determined using micro-FRNTs⁴⁴. Disease severity was classified according to World Health Organization criteria⁴⁵.

Identification of antigen-specific CD8⁺ T cells

Antigen-specific CD8⁺ T cells were labeled with optimal concentrations of the indicated HLA-A*11:01p tetramers (PE or APC) for 20 min at 37 °C, and then stained with the following monoclonal antibodies (mAbs) for 30 min at 4 °C: (i) α CD8-BV711 or α CD8-PerCP (BioLegend); (ii) α CD3-APC-H7, α CD14-V500, and α CD19-V500 (BD Biosciences); and, in some experiments, (iii) α TRBV11-2-FITC (Beckman Coulter). Non-viable events were excluded using Fixable Aqua or Violet Dead Cell Stain Kits (Thermo Fisher Scientific).

TCR clonotype analysis

Live CD3⁺CD8⁺CD14⁻CD19⁻ HLA-A*11:01p tetramer⁺ cells were sorted at > 98% purity directly into O-ring microtubes (Sarstedt) containing 100 μ L RNAlater (Applied Biosystems) using a custom-modified FACSAria II flow cytometer (BD Biosciences). Unbiased amplification of all expressed *TRB* gene products was conducted using a template-switch anchored RT-PCR as described previously⁴⁶. At least 50 functional sequences were

analyzed per sample. Gene usage was determined according to the ImMunoGeneTics (IMGT) nomenclature⁴⁷.

Generation and maintenance of CD8⁺ T cell clones

NS3₁₃₃ DENV-specific CD8⁺ T cell clones were derived from parental lines stained with serotype-matched HLA-A*11:01p tetramers. Single tetramer⁺ events were sorted by flow cytometry and amplified in RPMI-1640 containing 10% human serum, 100 U/mL penicillin G, 100 µg/mL streptomycin, and 2 mM L-glutamine, together with mixed irradiated PBMCs, 40 µg/mL phytohaemagglutinin, and 200 U/mL IL-2. Cells were restimulated every 2–3 weeks using the same protocol. Clonally expressed *TRA* and *TRB* gene rearrangements were analyzed as described previously⁴⁶.

Intracellular cytokine staining

Clonal CD8⁺ T cells were incubated with HLA-matched B-lymphoblastoid cells at a ratio of 1:1 for 5 hr in the absence or presence of 1 µg/mL peptide (as indicated), αCD107a-FITC (BD Biosciences), brefeldin A (10 µg/mL; Sigma-Aldrich), and GolgiStop (0.7 µL/mL; BD Biosciences). Non-viable events were excluded using a Fixable Violet Dead Cell Stain Kit (Thermo Fisher Scientific) prior to surface staining with αCD8-PerCP (BD Biosciences). Cells were then fixed/permeabilized with BD Cytofix/Cytoperm (BD Biosciences), washed with BD Perm/Wash Buffer (BD Biosciences), and stained intracellularly with the following mAbs: (i) αIFN-γ-APC-Cy7 and αTNF-α-PE-Cy7 (BioLegend); and (ii) αIL-2-APC and αMIP-1β-PE (BD Biosciences). Staphylococcal enterotoxin B (1 µg/mL; Sigma-Aldrich) was used as a positive control. Data were acquired using a FACSVerse flow cytometer (BD Biosciences) and analyzed with FlowJo software version 7.6.5 (Tree Star Inc.).

IFN-γ ELISpot assay

Clonal CD8⁺ T cells were incubated in duplicate with mock-treated or peptide-pulsed HLA-matched B-lymphoblastoid cells at a ratio of 1:8 for 12–16 hr in 96-well polyvinylidene difluoride-backed plates (Millipore) pre-coated with an α IFN- γ capture mAb (1-D1K; Mabtech). IFN- γ spots were revealed using an ELISpot Kit (Mabtech) and counted using an automated ELISpot plate reader (Autoimmun Diagnostika GmbH).

Tetramer dilution assay

Clonal CD8⁺ T cells were incubated with various concentrations of the indicated wild-type or mutant HLA-A*11:01p tetramers for 15 min at 37°C. Non-viable events were excluded using a Fixable Violet Dead Cell Stain Kit (Thermo Fisher Scientific) prior to surface staining with α CD8-APC (BD Biosciences). Data were acquired using an LSR Fortessa flow cytometer (BD Biosciences) and analyzed with FlowJo software version 7.6.5 (Tree Star Inc.).

Protein expression and purification

The D2H, D13, and D30 TCRs were expressed, refolded, and purified using an engineered disulfide linkage between the α and β constant domains⁴⁸. Soluble HLA-A*11:01 complexes incorporating the GTS1 (wild-type or mutant), GTS2, and GTS3/4 peptides were prepared as described previously^{49, 50}. Site-directed mutagenesis was used to introduce single residue substitutions (alanine or glycine) into the D30 TCR β -chain (n = 13) and the HLA-A*11:01 heavy chain (n = 7).

Thermal stability assay

HLA-A*11:01p stability was determined using a thermal shift assay with a real time detection system (Rotor-Gene 3000; Corbett Life Science). Two concentrations of each HLA-A*11:01p complex (5 and 10 μ M) were heated from 30 to 95 °C at a rate of 1 °C/min in 10 mM Tris-HCl pH 8 and 150 mM NaCl. Protein unfolding was monitored using the fluorescent dye Sypro Orange (Sigma-Aldrich). Fluorescence intensity was measured with excitation at 530

nm and emission at 555 nm. All experiments were performed in duplicate. The thermal melt point (T_M) represents the temperature at which 50% of the protein is unfolded.

Crystallization and structure determination

Crystals of HLA-A*11:01-GTS1 and HLA-A*11:01-GTS3/4, either free or in complex with the D30 TCR, were grown by the hanging-drop, vapour-diffusion method. The proteins were incubated at a concentration of 5 mg/mL in 10 mM Tris-HCl pH 8 and 150 mM NaCl at a temperature of 20 °C with a protein/reservoir drop ratio of 1:1. The HLA-A*11:01p complexes were crystallized in 1.4–1.8 M NH_4SO_4 , 0.2 M NaCl, 0.1 M Na cacodylate pH 6.5, and 2% ethylene glycol (EG). The TCR-HLA-A*11:01p complexes were crystallized in 17% polyethylene glycol (PEG) 8000, 2% EG, and 0.1 M HEPES pH 7.5. All crystals were soaked in a cryoprotectant solution containing mother liquor with the EG or PEG concentration increased to 30% (w/v), and then flash frozen in liquid nitrogen. Data were collected on the MX1 and MX2 beamlines at the Australian Synchrotron using the ADSC-Quantum 210 and 315r CCD detectors, respectively (at 100 K). Data were processed using XDS software⁵¹ and scaled using SCALA software⁵² from the CCP4 suite. Structures were determined by molecular replacement using the Phaser program⁵³, with the CF34 TCR as the search model for the D30 TCR (Protein Data Bank accession code, 3FFC)⁴⁸ and HLA-A*02:01 as the search model for peptide-free HLA-A*11:01 (Protein Data Bank accession code, 3GSO)⁵⁴. Manual model building was conducted using Coot software⁵⁵ followed by maximum-likelihood refinement with the Buster program (<http://www.globalphasing.com>). The TCR was numbered according to the IMGT unique numbering system⁴⁷, whereby the CDR1 loops start at residue number 27, the CDR2 loops start at residue number 56, and the CDR3 loops start at residue number 105. The final model was validated using Protein Data Bank software, and the final refinement statistics are summarized in Table 2. All molecular graphics representations were created using PyMol (<http://www.pymol.org>).

Surface plasmon resonance

TCR binding to HLA-A*11:01p complexes was quantified using surface plasmon resonance. All experiments were conducted at 25 °C on a BIAcore 3000 or T200 instrument (GE Healthcare) with TBS/BSA buffer (10 mM Tris-HCl pH 8, 150 mM NaCl, 0.005% surfactant P20, and 1% bovine serum albumin) as described previously⁴⁸. The D2H, D13, and D30 (wild-type and mutant) TCRs were immobilized separately on research-grade CM5 chips via a specific amine-coupled mAb⁵⁶. Each HLA-A*11:01p complex was then tested in duplicate over a fluid phase concentration range of 0.78–200 μ M (for the D2H TCR) or 1.56–400 μ M (for the D13, wild-type D30, and mutant D30 TCRs). Data were analyzed with BIAevaluation software version 3.1 using the 1:1 Langmuir binding model.

ACKNOWLEDGEMENTS

We thank Nattaya Tangthawornchaikul for management of the clinical database, Kristy Campbell, Hanim Halim, Andrea Nguyen, and staff at the Monash Macromolecular Crystallization Facility for technical support, and staff at the Australian Synchrotron for assistance with data collection. This work was funded by the Australian Research Council, the National Health and Medical Research Council, the National Institute for Health Research, the Thailand National Centre for Genetic Engineering and Biotechnology, the Thailand Tropical Disease Research Program T2, and the Wellcome Trust. SG is an Australian Research Council Future Fellow. JR is an Australian Laureate Fellow. DAP and GRS are Wellcome Trust Senior Investigators.

REFERENCES

1. Bhatt, S. *et al.* The global distribution and burden of dengue. *Nature* **496**, 504-507 (2013).
2. Sangkawibha, N. *et al.* Risk factors in dengue shock syndrome: a prospective epidemiologic study in Rayong, Thailand. I. The 1980 outbreak. *Am J Epidemiol* **120**, 653-669 (1984).
3. Guzman, M.G. *et al.* Epidemiologic studies on Dengue in Santiago de Cuba, 1997. *Am J Epidemiol* **152**, 793-799 (2000).
4. Halstead, S.B. Neutralization and antibody-dependent enhancement of dengue viruses. *Adv Virus Res* **60**, 421-467 (2003).
5. Morens, D.M., Larsen, L.K. & Halstead, S.B. Study of the distribution of antibody-dependent enhancement determinants on dengue 2 isolates using dengue 2-derived monoclonal antibodies. *J Med Virol* **22**, 163-167 (1987).
6. Littaua, R., Kurane, I. & Ennis, F.A. Human IgG Fc receptor II mediates antibody-dependent enhancement of dengue virus infection. *J Immunol* **144**, 3183-3186 (1990).
7. Marchette, N.J., Halstead, S.B., Falkler, W.A., Jr., Stenhouse, A. & Nash, D. Studies on the pathogenesis of dengue infection in monkeys. 3. Sequential distribution of virus in primary and heterologous infections. *J Infect Dis* **128**, 23-30 (1973).
8. Halstead, S.B., Shotwell, H. & Casals, J. Studies on the pathogenesis of dengue infection in monkeys. II. Clinical laboratory responses to heterologous infection. *J Infect Dis* **128**, 15-22 (1973).
9. Zellweger, R.M., Prestwood, T.R. & Shresta, S. Enhanced infection of liver sinusoidal endothelial cells in a mouse model of antibody-induced severe dengue disease. *Cell Host Microbe* **7**, 128-139 (2010).
10. Libraty, D.H. *et al.* Differing influences of virus burden and immune activation on disease severity in secondary dengue-3 virus infections. *J Infect Dis* **185**, 1213-1221 (2002).
11. Simmons, C.P. *et al.* Early T-cell responses to dengue virus epitopes in Vietnamese adults with secondary dengue virus infections. *J Virol* **79**, 5665-5675 (2005).
12. Duangchinda, T. *et al.* Immunodominant T-cell responses to dengue virus NS3 are associated with DHF. *Proc Natl Acad Sci U S A* **107**, 16922-16927 (2010).

13. Weiskopf, D. *et al.* Comprehensive analysis of dengue virus-specific responses supports an HLA-linked protective role for CD8+ T cells. *Proc Natl Acad Sci U S A* **110**, E2046-2053 (2013).
14. Zellweger, R.M. *et al.* Role of humoral versus cellular responses induced by a protective dengue vaccine candidate. *PLoS Pathog* **9**, e1003723 (2013).
15. Zellweger, R.M. *et al.* CD8+ T Cells Can Mediate Short-Term Protection against Heterotypic Dengue Virus Reinfection in Mice. *J Virol* **89**, 6494-6505 (2015).
16. Villar, L. *et al.* Efficacy of a tetravalent dengue vaccine in children in Latin America. *N Engl J Med* **372**, 113-123 (2015).
17. Chandanayingyong, D. *et al.* HLA-A, -B, -DRB1, -DQA1, and -DQB1 polymorphism in Thais. *Hum Immunol* **53**, 174-182 (1997).
18. Dung, N.T. *et al.* Timing of CD8+ T cell responses in relation to commencement of capillary leakage in children with dengue. *J Immunol* **184**, 7281-7287 (2010).
19. Mongkolsapaya, J. *et al.* Original antigenic sin and apoptosis in the pathogenesis of dengue hemorrhagic fever. *Nat Med* **9**, 921-927 (2003).
20. Bridgeman, J.S., Sewell, A.K., Miles, J.J., Price, D.A. & Cole, D.K. Structural and biophysical determinants of alphabeta T-cell antigen recognition. *Immunology* **135**, 9-18 (2012).
21. Rossjohn, J. *et al.* T cell antigen receptor recognition of antigen-presenting molecules. *Annu Rev Immunol* **33**, 169-200 (2015).
22. Beringer, D.X. *et al.* T cell receptor reversed polarity recognition of a self-antigen major histocompatibility complex. *Nat Immunol* **16**, 1153-1161 (2015).
23. Gras, S. *et al.* Reversed T Cell Receptor Docking on a Major Histocompatibility Class I Complex Limits Involvement in the Immune Response. *Immunity* **45**, 749-760 (2016).
24. Day, E.B. *et al.* Structural basis for enabling T-cell receptor diversity within biased virus-specific CD8+ T-cell responses. *Proc Natl Acad Sci U S A* **108**, 9536-9541 (2011).
25. Gras, S. *et al.* Allelic polymorphism in the T cell receptor and its impact on immune responses. *J Exp Med* **207**, 1555-1567 (2010).
26. Miles, J.J. *et al.* CTL recognition of a bulged viral peptide involves biased TCR selection. *J Immunol* **175**, 3826-3834 (2005).

27. Adams, J.J. *et al.* Structural interplay between germline interactions and adaptive recognition determines the bandwidth of TCR-peptide-MHC cross-reactivity. *Nat Immunol* **17**, 87-94 (2016).
28. Feng, D., Bond, C.J., Ely, L.K., Maynard, J. & Garcia, K.C. Structural evidence for a germline-encoded T cell receptor-major histocompatibility complex interaction 'codon'. *Nat Immunol* **8**, 975-983 (2007).
29. Stadinski, B.D. *et al.* A role for differential variable gene pairing in creating T cell receptors specific for unique major histocompatibility ligands. *Immunity* **35**, 694-704 (2011).
30. Loke, H. *et al.* Strong HLA class I--restricted T cell responses in dengue hemorrhagic fever: a double-edged sword? *J Infect Dis* **184**, 1369-1373 (2001).
31. Nguyen, T.P. *et al.* Protective and enhancing HLA alleles, HLA-DRB1*0901 and HLA-A*24, for severe forms of dengue virus infection, dengue hemorrhagic fever and dengue shock syndrome. *PLoS Negl Trop Dis* **2**, e304 (2008).
32. Appanna, R., Ponnampalavanar, S., Lum Chai See, L. & Sekaran, S.D. Susceptible and protective HLA class 1 alleles against dengue fever and dengue hemorrhagic fever patients in a Malaysian population. *PLoS One* **5**, e13029 (2010).
33. Malavige, G.N. *et al.* HLA class I and class II associations in dengue viral infections in a Sri Lankan population. *PLoS One* **6**, e20581 (2011).
34. Stephens, H.A. *et al.* HLA-A and -B allele associations with secondary dengue virus infections correlate with disease severity and the infecting viral serotype in ethnic Thais. *Tissue Antigens* **60**, 309-318 (2002).
35. Vejbaesya, S. *et al.* HLA Class I Supertype Associations With Clinical Outcome of Secondary Dengue Virus Infections in Ethnic Thais. *J Infect Dis* **212**, 939-947 (2015).
36. Kouri, G.P., Guzman, M.G., Bravo, J.R. & Triana, C. Dengue haemorrhagic fever/dengue shock syndrome: lessons from the Cuban epidemic, 1981. *Bull World Health Organ* **67**, 375-380 (1989).
37. Alvarez, M. *et al.* Dengue hemorrhagic Fever caused by sequential dengue 1-3 virus infections over a long time interval: Havana epidemic, 2001-2002. *Am J Trop Med Hyg* **75**, 1113-1117 (2006).
38. OhAinle, M. *et al.* Dynamics of dengue disease severity determined by the interplay between viral genetics and serotype-specific immunity. *Sci Transl Med* **3**, 114ra128 (2011).

39. Mongkolsapaya, J. *et al.* T cell responses in dengue hemorrhagic fever: are cross-reactive T cells suboptimal? *J Immunol* **176**, 3821-3829 (2006).
40. Chau, T.N. *et al.* Dengue in Vietnamese infants--results of infection-enhancement assays correlate with age-related disease epidemiology, and cellular immune responses correlate with disease severity. *J Infect Dis* **198**, 516-524 (2008).
41. Friberg, H. *et al.* Memory CD8+ T cells from naturally acquired primary dengue virus infection are highly cross-reactive. *Immunol Cell Biol* **89**, 122-129 (2011).
42. Yenchitsomanus, P.T. *et al.* Rapid detection and identification of dengue viruses by polymerase chain reaction (PCR). *Southeast Asian J Trop Med Public Health* **27**, 228-236 (1996).
43. Innis, B.L. *et al.* An enzyme-linked immunosorbent assay to characterize dengue infections where dengue and Japanese encephalitis co-circulate. *Am J Trop Med Hyg* **40**, 418-427 (1989).
44. Jirakanjanakit, N., Sanohsomneing, T., Yoksan, S. & Bhamarapavati, N. The micro-focus reduction neutralization test for determining dengue and Japanese encephalitis neutralizing antibodies in volunteers vaccinated against dengue. *Trans R Soc Trop Med Hyg* **91**, 614-617 (1997).
45. Dengue haemorrhagic fever: diagnosis, prevention, treatment and control. Geneva: World Health Organization; 1997.
46. Quigley, M.F., Almeida, J.R., Price, D.A. & Douek, D.C. Unbiased molecular analysis of T cell receptor expression using template-switch anchored RT-PCR. *Curr Protoc Immunol* **Chapter 10**, Unit10 33 (2011).
47. Lefranc, M.P. *et al.* IMGT, the international ImMunoGeneTics information system. *Nucleic Acids Res* **33**, D593-597 (2005).
48. Gras, S. *et al.* The shaping of T cell receptor recognition by self-tolerance. *Immunity* **30**, 193-203 (2009).
49. Clements, C.S. *et al.* The production, purification and crystallization of a soluble heterodimeric form of a highly selected T-cell receptor in its unliganded and liganded state. *Acta Crystallogr D Biol Crystallogr* **58**, 2131-2134 (2002).
50. Reid, S.W. *et al.* Production and crystallization of MHC class I B allele single peptide complexes. *FEBS Lett* **383**, 119-123 (1996).

51. Kabsch, W. Xds. *Acta Crystallogr D Biol Crystallogr* **66**, 125-132 (2010).
52. Evans, P. Scaling and assessment of data quality. *Acta Crystallogr D Biol Crystallogr* **62**, 72-82 (2006).
53. Read, R.J. Pushing the boundaries of molecular replacement with maximum likelihood. *Acta Crystallogr D Biol Crystallogr* **57**, 1373-1382 (2001).
54. Gras, S. *et al.* Structural bases for the affinity-driven selection of a public TCR against a dominant human cytomegalovirus epitope. *J Immunol* **183**, 430-437 (2009).
55. Emsley, P. & Cowtan, K. Coot: model-building tools for molecular graphics. *Acta Crystallogr D Biol Crystallogr* **60**, 2126-2132 (2004).
56. Borg, N.A. *et al.* The CDR3 regions of an immunodominant T cell receptor dictate the 'energetic landscape' of peptide-MHC recognition. *Nat Immunol* **6**, 171-180 (2005).

FIGURE LEGENDS

Figure 1 TRBV bias in NS3₁₃₃ DENV-specific CD8⁺ T cell populations. **(a)** The most common serotype-defined variants of the NS3₁₃₃ DENV epitope in viral isolates from Thailand. Amino acid mutations are underlined. The epitope sequences from DENV3 and DENV4 are identical (GTS3/4). *Frequency as reported by the National Center for Biotechnology Information. **(b)** Representative flow cytometry data showing HLA-A*11:01p tetramer reactivity patterns in venous blood samples from patients with primary or secondary DENV infection. Plots are gated on CD3⁺CD14⁻CD19⁻ events (left) or CD3⁺CD8⁺CD14⁻CD19⁻ events (middle and right). **(c)** Pie charts depicting concatenated TRBV transcript frequencies across all patients for the indicated CD3⁺CD8⁺CD14⁻CD19⁻ HLA-A*11:01p tetramer⁺ populations. SP, single positive; DP, double positive; 3, 3/4 (pie legends). **(d)** Representative flow cytometry data showing TRBV11-2 expression versus HLA-A*11:01p tetramer reactivity in venous blood samples from patients with secondary DENV infection. Plots are gated on CD8⁺ events. **(e)** TRBV11-2 expression frequency (%) within the indicated CD8⁺ HLA-A*11:01p tetramer⁺ populations. Each symbol represents one patient with secondary DENV infection. * $P < 0.05$ (Mann-Whitney U test).

Figure 2 Characterization of NS3₁₃₃ DENV-specific CD8⁺ T cell clones and the binary structures of HLA-A*11:01-GTS1 and HLA-A*11:01-GTS3/4. **(a)** Effector function profiles for the indicated NS3₁₃₃ DENV-specific CD8⁺ T cell clones stimulated with GTS1, GTS2, or GTS3/4. The negative control is shown in each case (medium alone). Five readouts were measured by flow cytometry (CD107a, MIP-1 β , TNF- α , IFN- γ , and IL-2). Data represent two independent experiments. Pie chart segments depict the fraction of cells expressing the number of functions indicated in the key. **(b)** TCR α and TCR β sequences expressed by clones OX17H 2H (D2H), 44-173 13 (D13), and 44-173 30 (D30). **(c)** The binary structure of HLA-A*11:01 (white cartoon) in complex with GTS1 (blue stick). **(d)** The binary structure of

HLA-A*11:01 (white cartoon) in complex with GTS3/4 (purple stick). **(e)** Superposition of the structures in (c) and (d).

Figure 3 Structures of the D30 TCR bound to HLA-A*11:01-GTS1 and HLA-A*11:01-GTS3/4. **(a)** The overall D30 TCR-HLA-A*11:01-GTS1 complex (top) with atomic footprints on the surface of HLA-A*11:01-GTS1 (bottom; HLA-A*11:01, white surface; GTS1, gray surface). **(b)** The overall D30 TCR-HLA-A*11:01-GTS3/4 complex (top) with atomic footprints on the surface of HLA-A*11:01-GTS3/4 (bottom; HLA-A*11:01, white surface; GTS3/4, gray surface). The pie charts depict the relative contributions of each D30 TCR segment to the interaction with each HLA-A*11:01p complex. Top: TCR α , light pink; TCR β , pale blue; HLA-A*11:01, gray; GTS1, black stick; GTS3/4, magenta stick. Bottom: CDR1 α , teal; CDR2 α , green; CDR3 α , purple; CDR1 β , red; CDR2 β , orange; CDR3 β , yellow; FW β , pale blue. Black spheres represent the mass center of V α and V β .

Figure 4 Interactions between the D30 TCR and HLA-A*11:01-GTS1. **(a)** Interaction between the CDR1 α loop (teal) and HLA-A*11:01 (gray). The peptide is depicted in black, with the C α of P1-Gly as a sphere. **(b)** Interaction between the CDR3 α loop (purple) and residues in the α 1-helix of HLA-A*11:01 (gray). **(c)** The CDR2 β loop (orange) and FW β (pale blue) are positioned above a long stretch of the HLA-A*11:01 α 1-helix (gray). **(d)** The CDR3 β loop (yellow) bridges the antigen-binding cleft to contact both helices of HLA-A*11:01 (gray). **(e, f)** The GTS1 peptide (black) is mainly contacted by the CDR3 β loop (yellow) and the CDR2 β loop (orange). Red dashed lines represent hydrogen bonds, and blue dashed lines represent van der Waals contacts.

Figure 5 Asn58 β usage in NS3₁₃₃ DENV-specific CD8⁺ T cell populations. **(a)** Pie charts depicting concatenated frequencies of Asn58 β ⁺ (purple and cyan) and Asn58 β ⁻ (orange) TRBV segments across all patients for the indicated CD3⁺CD8⁺CD14⁻CD19⁻ HLA-A*11:01p

tetramer⁺ populations. The Asn58 β ⁺ TRBV segments are subdivided according to the absence (purple) or presence (cyan) of a charged residue at position 59. **(b)** Individual TRBV frequencies and associated CDR2 β sequences in the same dataset. The highest frequencies are shown in blue for each CD3⁺CD8⁺CD14⁻CD19⁻ HLA-A*11:01p tetramer⁺ population (GTS1, GTS2, and GTS3/4). The conserved Asn58 β residue is highlighted in red, and the charged residues at position 59 are highlighted in cyan (CDR2 β).

Figure 6 Energetic hotspot analysis of TRBV11-2⁺ TCR interactions with HLA-A*11:01-GTS1. **(a)** Energetic footprint on the D30 TCR. Mutated residues are colored to indicate effects on the D30 TCR interaction with HLA-A*11:01-GTS1: yellow, minimal impact (< 3-fold change in affinity); orange, moderate impact (3–5-fold decrease in affinity); red, critical impact (> 5-fold decrease in affinity); blue, positive impact (> 3-fold increase in affinity). TCR α , pale pink; TCR β , pale blue. **(b)** Energetic footprint on HLA-A*11:01 (white surface) complexed with GTS1 (gray surface) for the D30 TCR. Mutated residues are colored as in panel (a). **(c)** Energetic footprint on HLA-A*11:01 (white surface) complexed with GTS1 (gray surface) for the D13 TCR. Mutated residues are colored as in panel (a). **(d)** Energetic footprint on HLA-A*11:01 (white surface) complexed with GTS1 (gray surface) for the D2H TCR. Mutated residues are colored as in panel (a). **(e)** Detail of the critical interaction between Asn58 β (CDR2 β) and P9-Asn (GTS1). Residues are colored as in panel (a). **(f)** Functional sensitivity of the NS3₁₃₃ DENV-specific CD8⁺ T cell clones 44-173 13 (D13) and 44-173 30 (D30) for the indicated GTS1 mutant peptides. The TRBV7-6⁺ NS3₁₃₃ DENV-specific CD8⁺ T cell clone E5 was included as a control. EC₅₀ values represent the peptide concentration required to elicit a half-maximal response in IFN- γ ELISpot assays (μ g/mL). Data represent three independent experiments. Yellow, minimal impact (< 5-fold change in EC₅₀); red, critical impact (> 10-fold increase in EC₅₀).

TCR	GTS1	GTS2	GTS3/4
D2H	7.35 ± 0.90 μM	> 200 μM	9.75 ± 0.13 μM
D13	> 400 μM	> 400 μM	> 400 μM
D30	136.0 ± 7.0 μM	> 400 μM	142.5 ± 2.5 μM

Representative surface plasmon resonance data are shown in Supplementary Figure 7. The listed K_{Deq} values were averaged over three independent experiments carried out in duplicate (mean ± SEM).

Table 1 Equilibrium binding affinities of soluble HLA-A*11:01-GTS1, HLA-A*11:01-GTS2, and HLA-A*11:01-GTS3/4 complexes to the D2H, D13, and D30 TCRs.

	TCR-HLA-A*11:01-GTS1	TCR-HLA-A*11:01-GTS3/4	HLA-A*11:01-GTS1	HLA-A*11:01-GTS3/4
Data collection				
Space group	<i>P</i> 2 ₁ 2 ₁ 2 ₁	<i>P</i> 2 ₁	<i>C</i> 2	<i>C</i> 2
Cell dimensions				
a, b, c (Å)	88.06, 146.38, 167.56	77.39, 170.54, 85.69	155.50, 150.20, 105.83	158.32, 145.52, 106.30
α, β, γ (°)		β = 113.89	β = 120.53	β = 121.14
Resolution (Å)	47.17 – 2.95 (3.05 – 2.95)	46.01 – 3.20 (3.37 – 3.20)	49.09 – 3.15 (3.32 – 3.15)	48.97 – 2.85 (3.00 – 2.85)
Total no. of observations	396406 (39145)	122531 (17850)	154836 (22722)	179270 (27072)
No. of unique observations	46399 (4499)	33473 (4865)	36207 (2578)	47263 (7023)
Multiplicity	8.5 (8.7)	3.7 (3.7)	4.3 (4.3)	6.7 (2.1)
Data completeness (%)	100.0 (100.0)	99.8 (99.9)	99.9 (99.9)	98.2 (100.0)
<i>I</i> /σ _{<i>i</i>}	7.2 (2.0)	6.7 (2.7)	14.8 (1.9)	6.7 (2.1)
R _{pim} ^a (%)	11.3 (48.2)	13.1 (36.4)	5.4 (44.6)	8.8 (35.3)
Refinement				
Non-hydrogen atoms				
Protein	13216	13217	9426	9439
Water	364	2	91	339
<i>R</i> _{factor} ^b (%)	18.9	17.5	17.70	20.05
<i>R</i> _{free} ^b (%)	25.4	24.6	23.07	22.99
Rmsd from ideality				
Bond lengths (Å)	0.007	0.008	0.010	0.007
Bond angles (°)	1.02	1.09	1.224	0.99
Ramachandran plot (%)				
Favored	95.1	92.4	90.8	96.4
Allowed	5.0	6.5	7.9	3.1
Disallowed	0.9	1.1	1.3	0.5

^aR_{pim} = $\sum_{hkl} [1/(N-1)]^{1/2} \sum_i |I_{hkl,i} - \langle I_{hkl} \rangle| / \sum_{hkl} \langle I_{hkl} \rangle$. ^bR_{factor} = $\sum_{hkl} ||F_o| - |F_c|| / \sum_{hkl} |F_o|$ for all data except ~ 5%, which were used for R_{free} calculation. Values in parentheses refer to the highest resolution bin for each dataset.

Table 2 Data collection and refinement statistics for the structure of HLA-A*11:01 presenting GTS1 or GTS3/4, either free or bound to the D30 TCR.

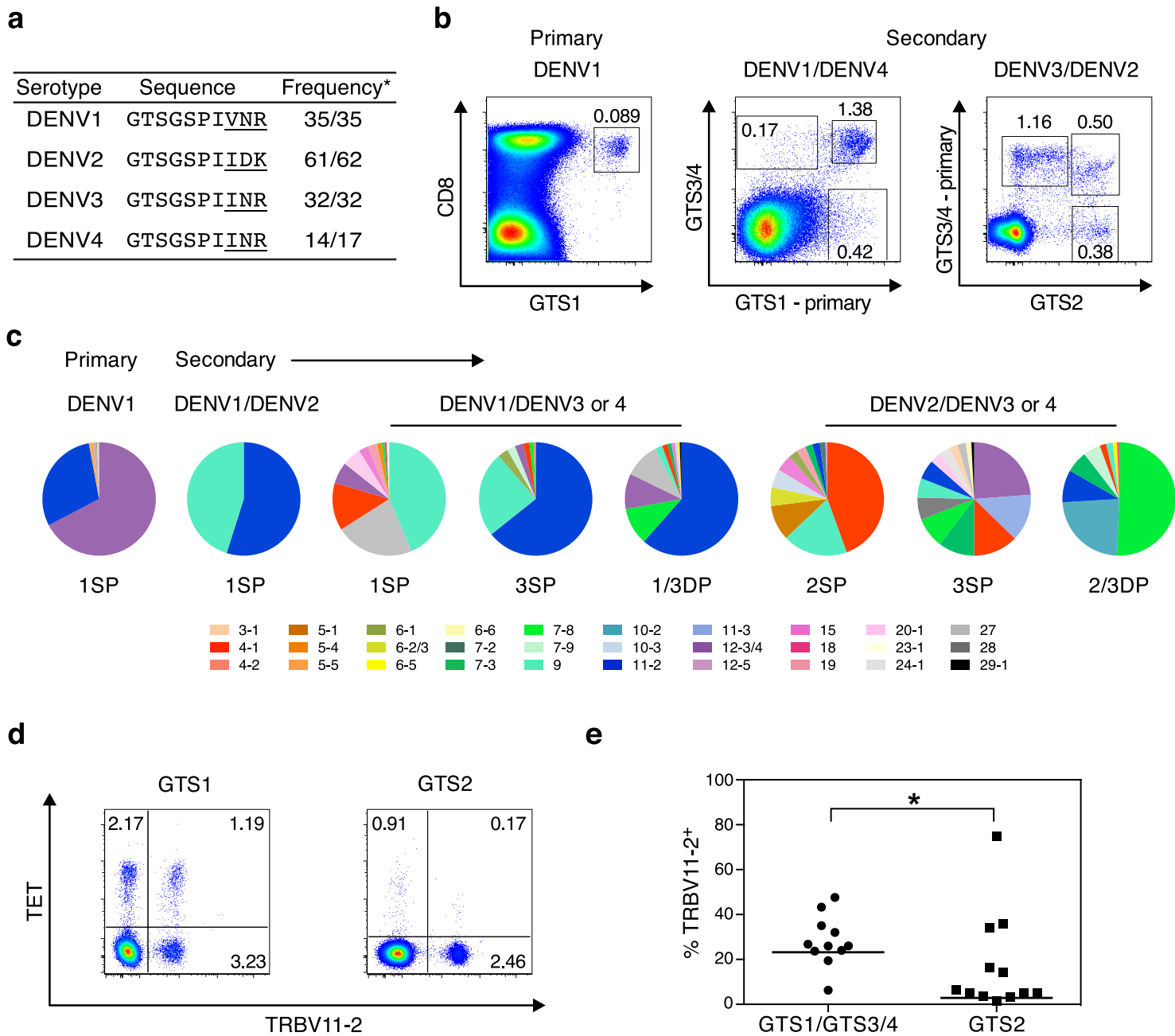
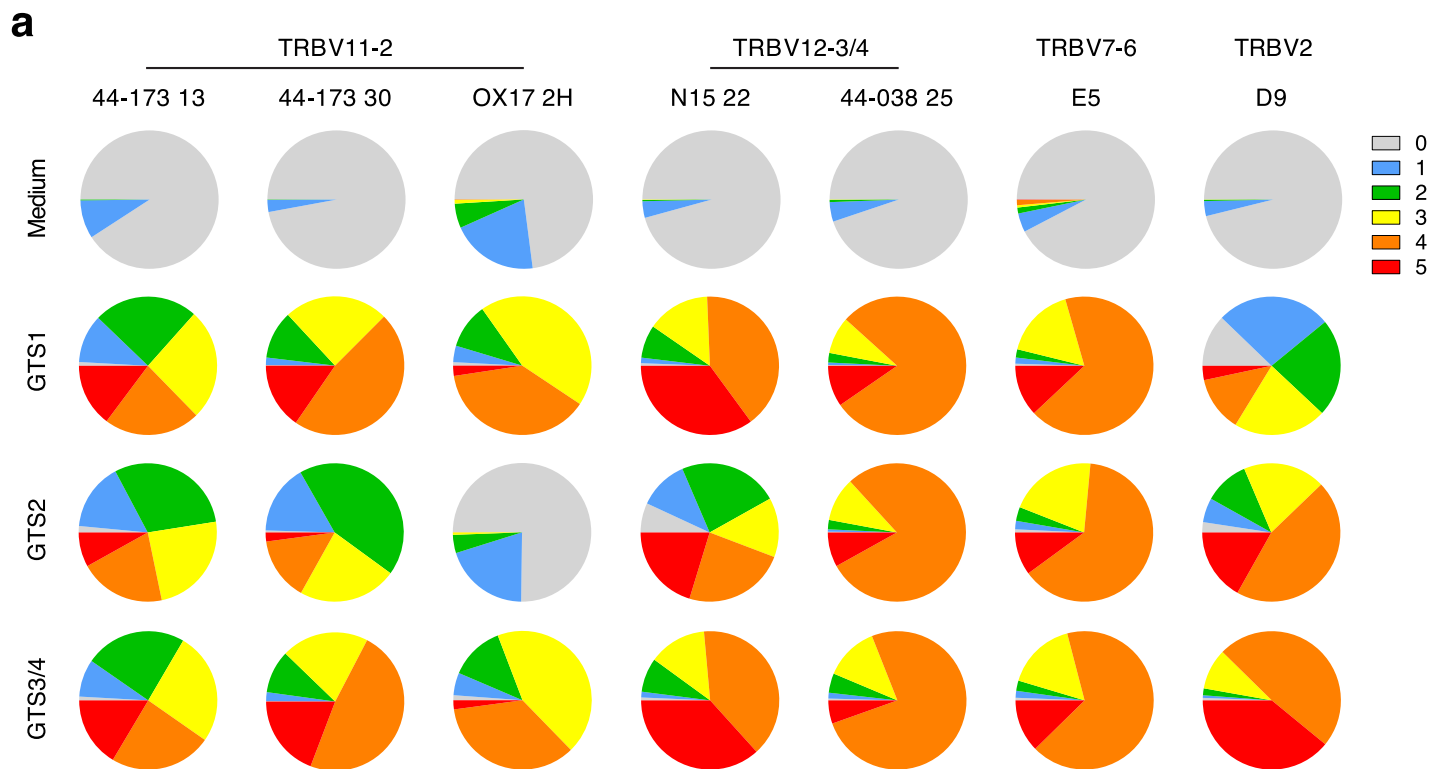


Figure 1



b

OX17 2H			44-173 13			44-173 30		
TRBV	CDR3 β	TRBJ	TRBV	CDR3 β	TRBJ	TRBV	CDR3 β	TRBJ
11-2	CASTTGGGGYEYQ	2-7	11-2	CASSLGQGSYEYQ	2-7	11-2	CASSLGQLLYGYT	1-2
TRAV	CDR3 α	TRAJ	TRAV	CDR3 α	TRAJ	TRAV	CDR3 α	TRAJ
9-2	CALDSGNTGKLI	37	8-2	CWSPFGNEKLT	48	30	CGLGDAGNMLT	39

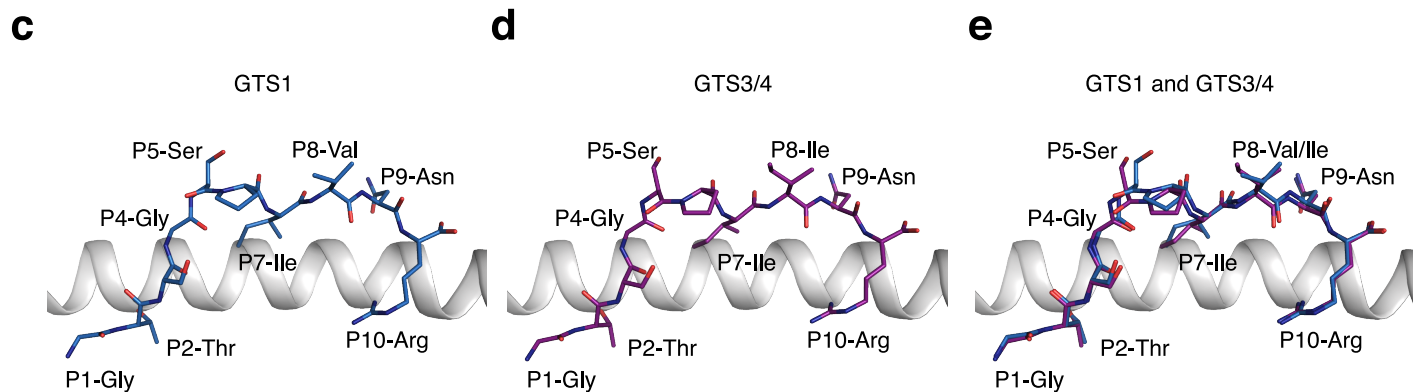


Figure 2

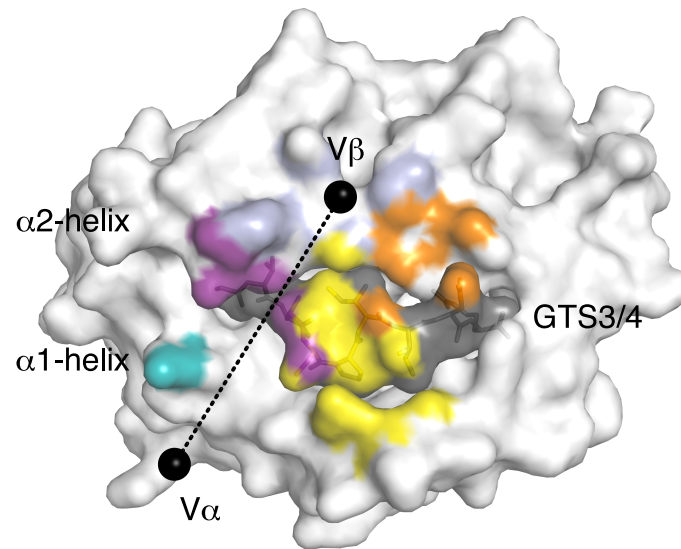
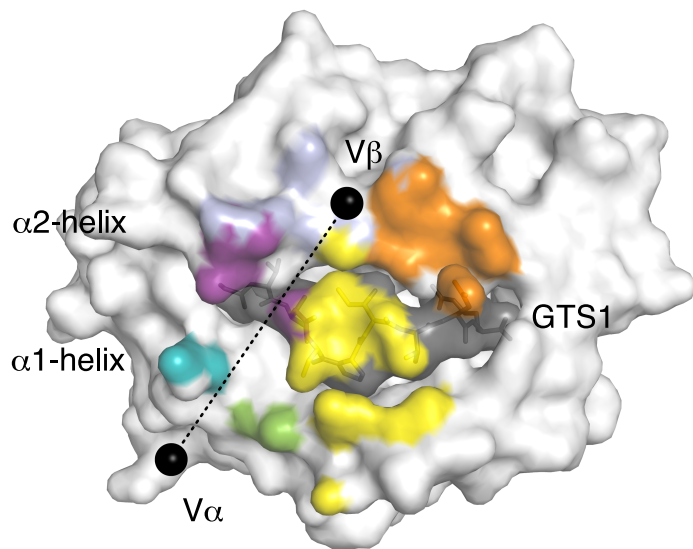
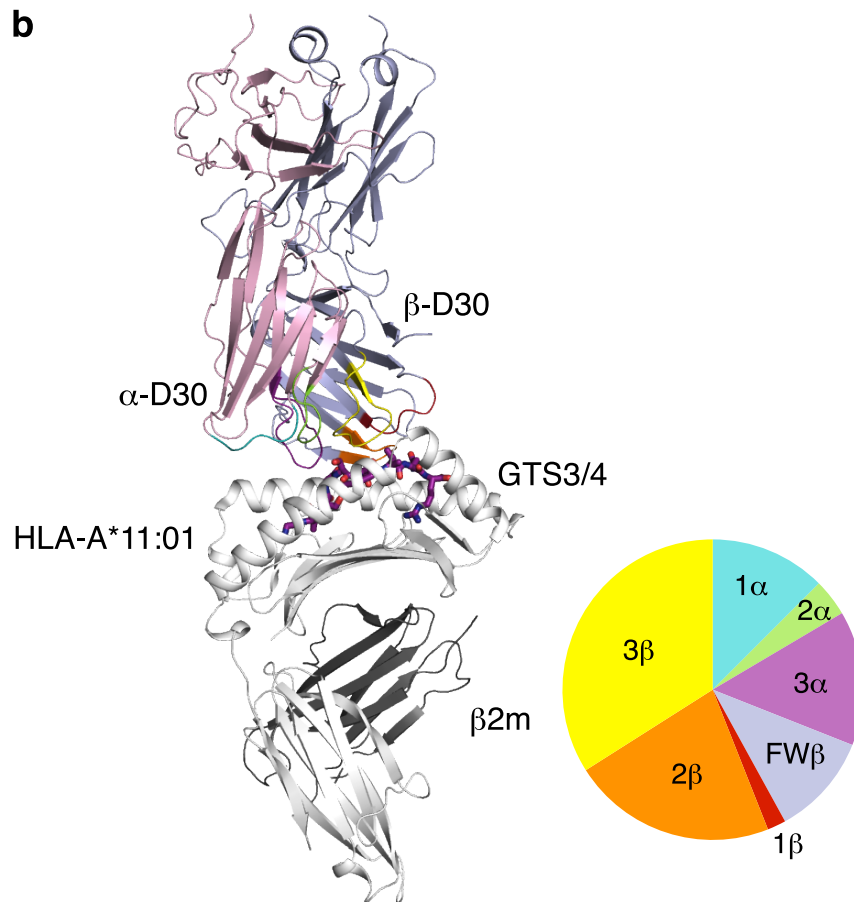
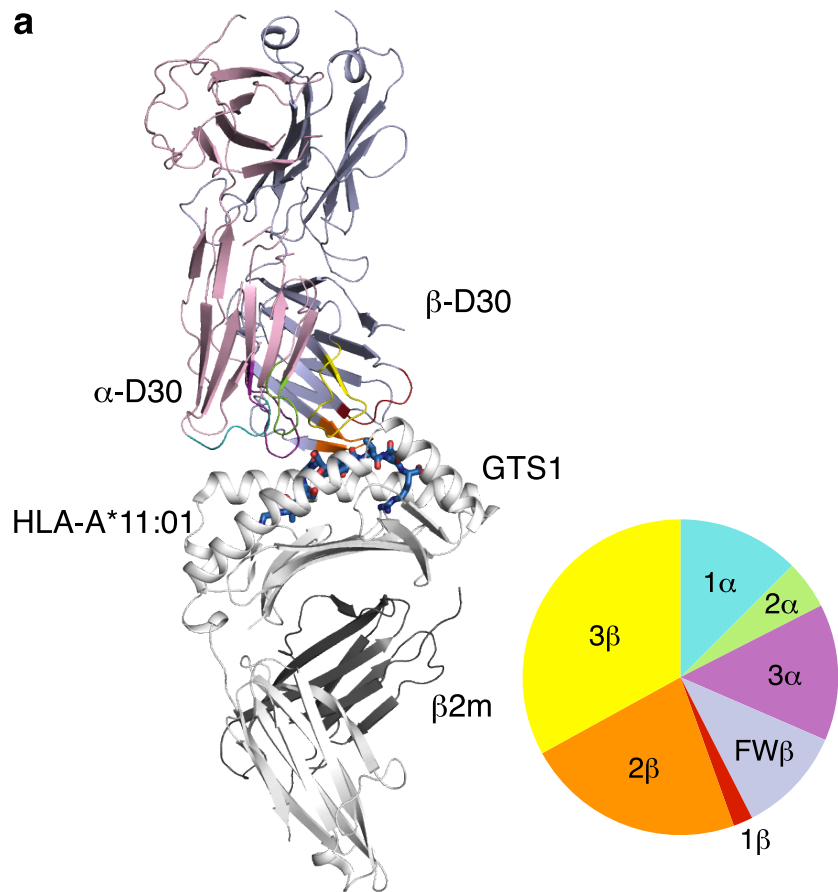
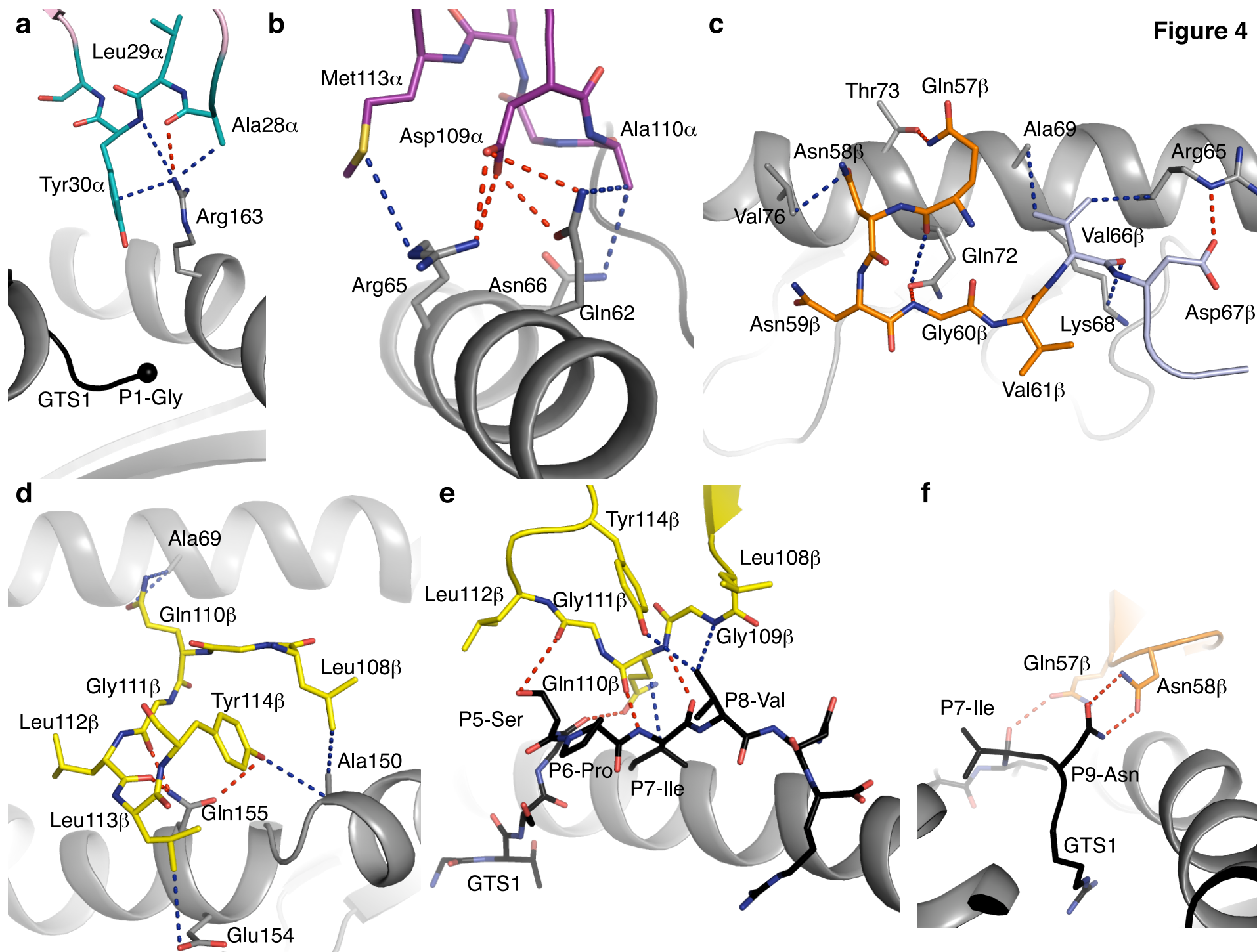
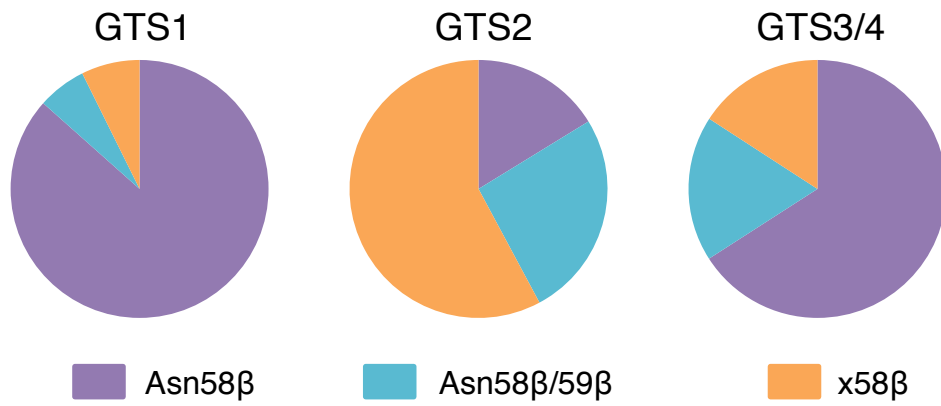


Figure 3

Figure 4

a



b

	CDR2β	TRBV	GTS1	GTS2	GTS3/4
Asn58β	YYNGEE	9	12.11	10.83	7.08
	FQ N NGV	11-2	38.76	5.41	45.50
	F N NNVP	12-3/4	28.38	0	8.40
	SM N VEV	27	7.32	0	4.92
Asn58β/59β	Y N NKEL	3-1	0.41	0	0.36
	FQ N EAQ	7-8	5.09	23.36	16.21
	FQ N EAQ	7-9	0	2.28	1.44
	Y E NEEA	11-3	0.20	0	0.24
	FR N RAP	12-5	0.31	0.28	0
	FQ N EQV	23-1	0.10	0	0
x58β	YSYEKL	4-1	2.64	24.79	3.36
	YNFKEQ	4-2	0	0	0.12
	YFSETQ	5-1	0	5.41	0
	YYREEE	5-4	0.20	0	0
	YYEKEE	5-5	0.41	0	0
	SASEGT	6-1	0.10	1.42	0.60
	SVGEGT	6-2	0	2.85	0
	SVGAGI	6-5	0.20	0.57	0.48
	SVGAGI	6-6	0	0	0.24
	FQGNSA	7-2	0	0.85	0
	FQGTGA	7-3	1.02	3.99	3.24
	SAAADI	10-2	0	10.82	4.56
	SYGVKD	10-3	0.31	2.85	0.36
	YYDKDF	15	0.81	2.56	0.48
	LQKENI	18	0.10	0.28	0.12
	SQIVND	19	0.41	1.42	0
	SNEGSKA	20-1	0.92	0	0.48
	SFDVKD	24-1	0	0	0.48
SYDVKM	28	0.20	0	1.20	
ANQGSEA	29-1	0	0	0.12	

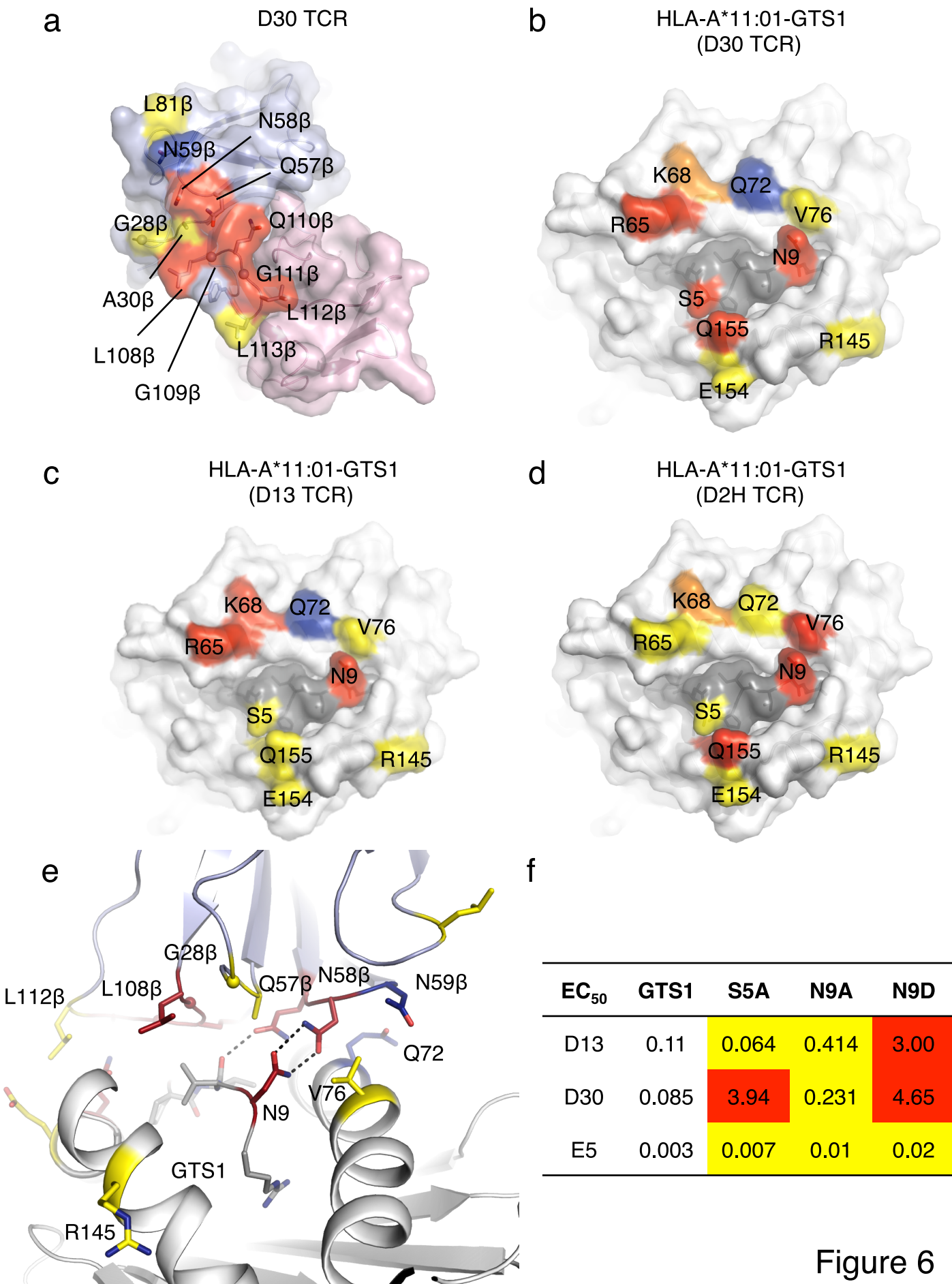


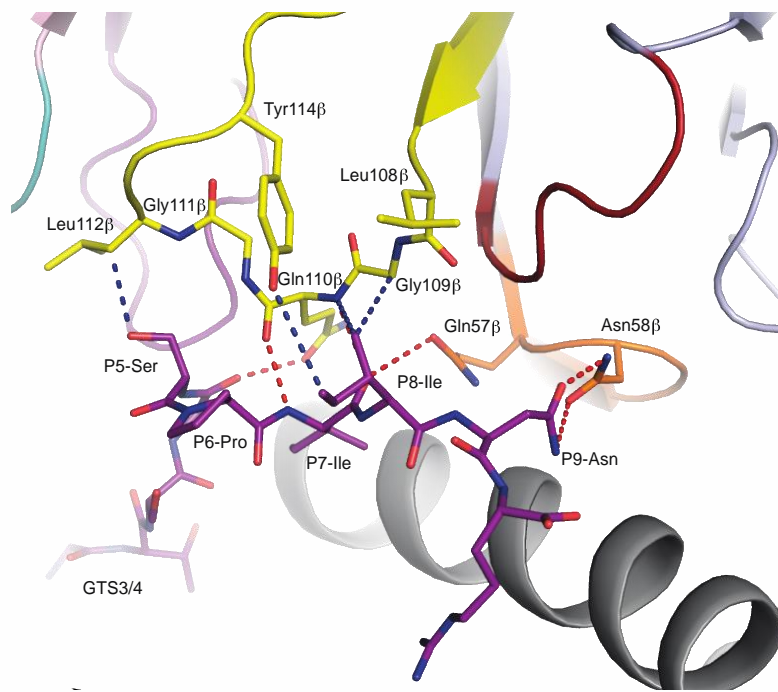
Figure 6

Sample ID	Sequence alignment
2-167-2 GTS3/4	C A S S L G P D S P L H
2-644-9 GTS1 + GTS3/4	tgtgccagcagcctcggaccggattcaccctccac
2-0600-8 GTS1	-----t-g--g--c----- -----t-a-----
Sample ID	Sequence alignment
2-278-1 GTS1	C A S S L G Q G A Y E Q Y
2-644-9 GTS1 + GTS3/4	tgtgccagcagccttggacagggcctacgagcagtac
2-162-9 GTS1 + GTS3/4	-----a-----g-----
2-162-9 GTS1 + GTS3/4	-----t-g-----c----- -----t-a-----g-----
Sample ID	Sequence alignment
1-1166-6 GTS1	C A S S L G A G E L F
2-1710-2 GTS1 + GTS3/4	tgtgccagcagtttaggtgccggggagctgttt
	-----cc-----
Sample ID	Sequence alignment
2-573-8 GTS3/4	C A S S L G P D Y E Q Y
2-162-9 GTS3/4	tgtgccagcagcctcggacctgactacgagcagtac
	-----t-a--g--a-----
Sample ID	Sequence alignment
2-278-1 GTS1	C A S S L G P D N E Q F
2-644-9 GTS1 + GTS3/4	tgtgccagcagcctcggacccgacaatgagcagttc
2-088-5 GTS3/4	-----t-g----g----- -----t-g-----
Sample ID	Sequence alignment
2-162-9 GTS1 + GTS3/4	C A S S L G G D T Y E Q Y
2-644-9 GTS1 + GTS3/4	tgtgccagcagccttagggggacacctacgagcagtac
	-----g-----
Sample ID	Sequence alignment
2-162-9 GTS1 + GTS3/4	C A S S L G G T D N E Q F
2-644-9 GTS1 + GTS3/4	tgtgccagcagccttaggtgggaccgacaatgagcagttc
	-----g--t--t-----
Sample ID	Sequence alignment
2-088-5 GTS2 + GTS3/4	C A S S Y R G G R A G E T Q Y
2-088-5 GTS2 + GTS3/4	tgtgccagcagttaccggggcgggagggccggcgagaccagtac
2-1710-2 GTS1 + GTS3/4	-----a----- -----a-----g-----

Supplementary Figure 1

CDR3 β nucleotide alignments for public NS3₁₃₃ DENV-specific TCRs.

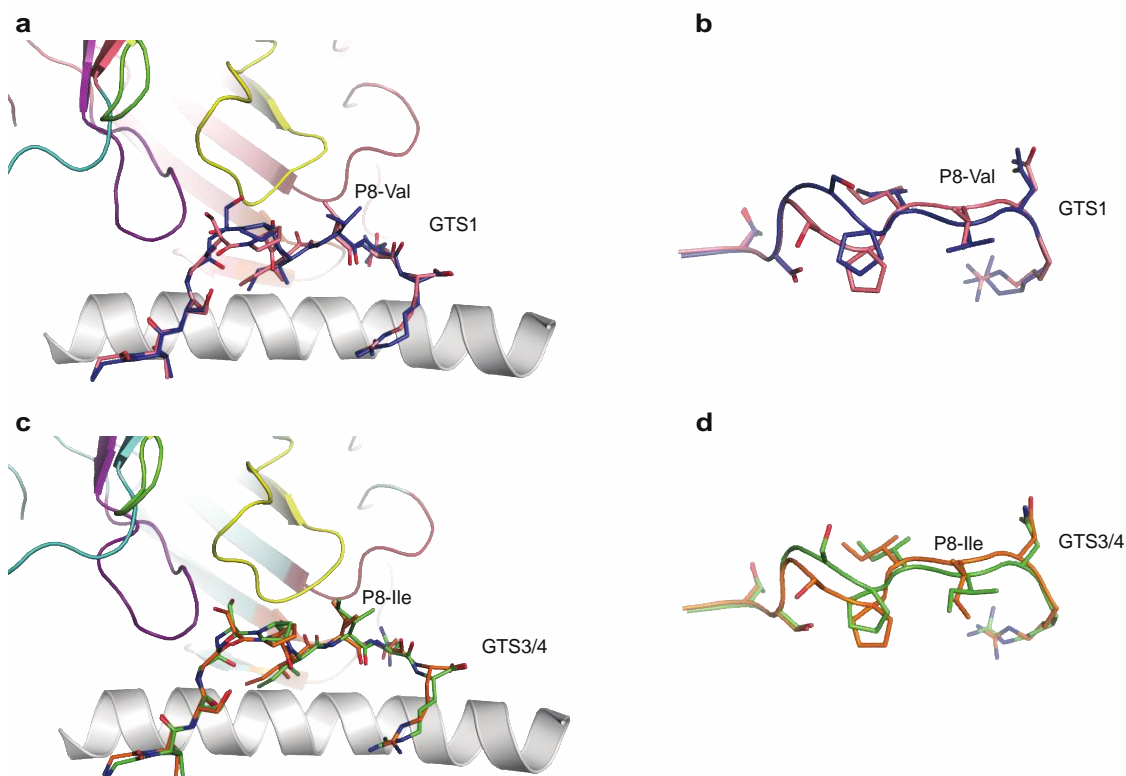
Nucleotide alignments for the indicated public CDR3 β amino acid sequences. Donor origin and HLA-A*11:01p tetramer specificity are indicated in the left column (see also Supplementary Table 2).



Supplementary Figure 2

Interactions between the D30 TCR and HLA-A*11:01-GTS3/4.

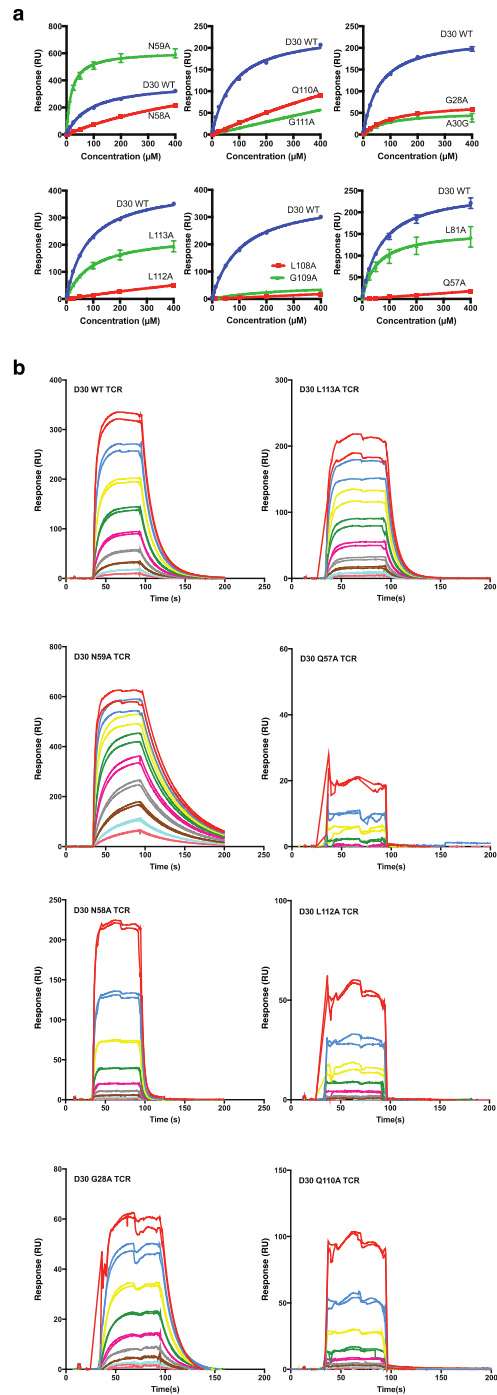
The GTS3/4 peptide (purple) is mainly contacted by the CDR3 β loop (yellow) and the CDR2 β loop (orange). Red dashed lines represent hydrogen bonds, and blue dashed lines represent van der Waals contacts.



Supplementary Figure 3

Structural comparison of free and bound NS3₁₃₃ DENV peptides in complex with HLA-A*11:01.

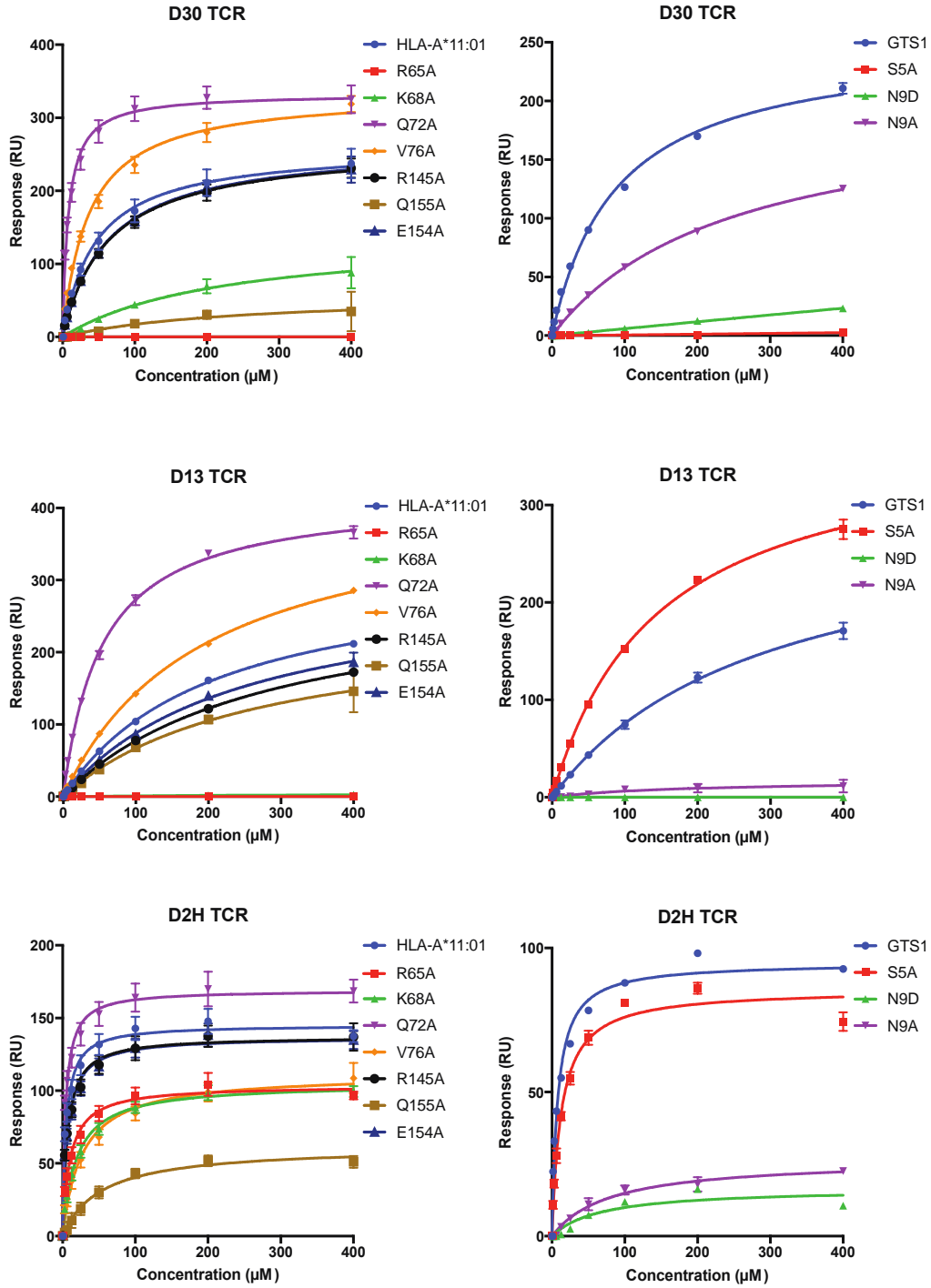
(a) Superposition of HLA-A*11:01-GTS1 free (pink stick) and bound to the D30 TCR (blue stick). HLA-A*11:01 is represented in white cartoon. The D30 TCR is represented in pink cartoon with the CDR loops colored as follows: CDR1α, teal; CDR2α, green; CDR3α, purple; CDR1β, red; CDR2β, orange; CDR3β, yellow. **(b)** Top view of panel (a) showing the peptide alone. **(c)** Superposition of HLA-A*11:01-GTS3/4 free (green stick) and bound to the D30 TCR (orange stick). HLA-A*11:01 is represented in white cartoon. The D30 TCR is represented in pink cartoon with the CDR loops colored as in panel (a). **(d)** Top view of panel (c) showing the peptide alone.



Supplementary Figure 4

Equilibrium binding of soluble HLA-GTS1 complexes to wild-type and mutant D30 TCRs.

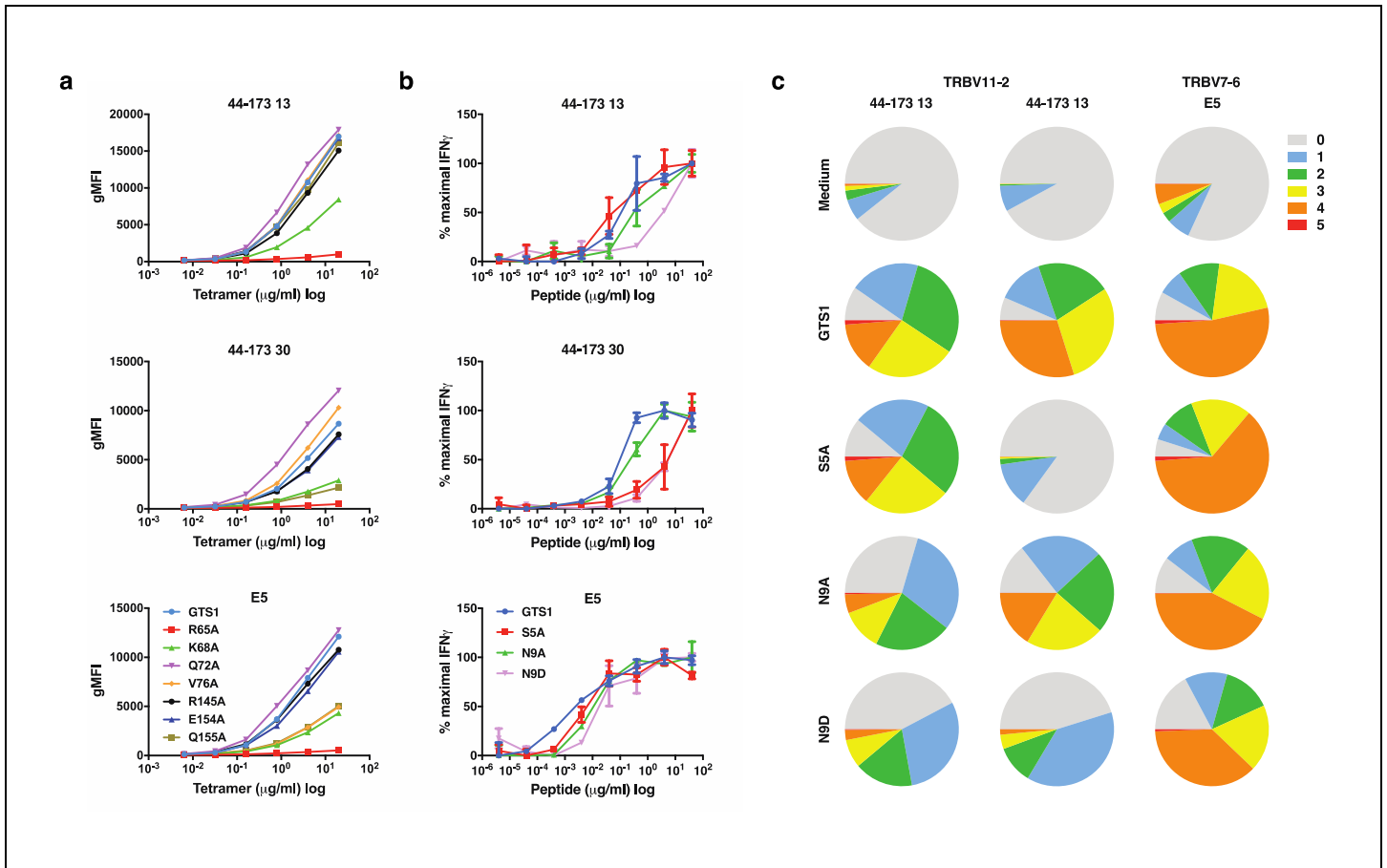
(a) Representative surface plasmon resonance data are shown for the indicated wild-type (WT) and mutant D30 TCRs. Two independent experiments were carried out in duplicate. Error bars indicate mean \pm SEM. (b) Representative surface plasmon resonance sensorgrams are shown for the indicated wild-type (WT) and mutant D30 TCRs. Colors indicate different concentrations (1.56–400 μ M) of the fluid phase analyte (HLA-A*11:01-GTS1).



Supplementary Figure 5

Equilibrium binding of soluble wild-type and mutant HLA-GTS1 complexes to the D2H, D13, and D30 TCRs.

Representative surface plasmon resonance data are shown for the indicated wild-type (WT) and mutant HLA-A*11:01-GTS1 complexes. Top: D30 TCR; middle; D13 TCR; bottom: D2H TCR. Two independent experiments were carried out in duplicate. Error bars indicate mean \pm SEM.



Supplementary Figure 6

Recognition of HLA-A*11:01 and GTS1 mutants by NS3₁₃₃ DENV-specific CD8⁺ T cell clones.

(a) Avidity of the NS3₁₃₃ DENV-specific CD8⁺ T cell clones 44-173 13 (D13) and 44-173 30 (D30) for the indicated wild-type and mutant HLA-A*11:01-GTS1 tetramers. The TRBV7-6⁺ NS3₁₃₃ DENV-specific CD8⁺ T cell clone E5 was included as a control. Data represent three independent experiments. Error bars indicate SD. gMFI, geometric mean fluorescence intensity. (b) Functional sensitivity of the NS3₁₃₃ DENV-specific CD8⁺ T cell clones 44-173 13 (D13) and 44-173 30 (D30) for the indicated wild-type and mutant GTS1 peptides in IFN- γ ELISpot assays. The TRBV7-6⁺ NS3₁₃₃ DENV-specific CD8⁺ T cell clone E5 was included as a control. Data represent three independent experiments. Error bars indicate SD. (c) Effector function profiles for the NS3₁₃₃ DENV-specific CD8⁺ T cell clones 44-173 13 (D13) and 44-173 30 (D30) stimulated with the indicated wild-type and mutant GTS1 peptides. The TRBV7-6⁺ clone E5 was included as a control. Five readouts were measured by flow cytometry (CD107a, MIP-1 β , TNF- α , IFN- γ , and IL-2). Data represent two independent experiments. Pie chart segments depict the fraction of cells expressing the number of functions indicated in the key.